

**ENHANCEMENT OF REACTIVE OXYGEN SPECIES PRODUCTION IN  
NANOPARTICULATE BIMETALLIC ZERO-VALENT IRON AND DIOXYGEN  
SYSTEM**

by  
Ivan Morales Parra

A thesis submitted in partial fulfillment of the requirements for the degree of

MASTER OF SCIENCE  
in  
CIVIL ENGINEERING

UNIVERSITY OF PUERTO RICO  
MAYAGÜEZ CAMPUS  
2010

Approved by:

\_\_\_\_\_  
Sangchul Hwang, Ph.D.  
President, Graduate Committee

\_\_\_\_\_  
Date

\_\_\_\_\_  
Jorge Rivera Santos, Ph.D.  
Member, Graduate Committee

\_\_\_\_\_  
Date

\_\_\_\_\_  
Yang Deng, Ph.D.  
Member, Graduate Committee

\_\_\_\_\_  
Date

\_\_\_\_\_  
Oscar Marcelo Suarez, Ph.D.  
Representative of Graduate Studies

\_\_\_\_\_  
Date

\_\_\_\_\_  
Ismael Pagán Trinidad, M.S.C.E.  
Chairperson of the Department

\_\_\_\_\_  
Date

## ABSTRACT

An emerging remediation process involving nanoscale zero-valent iron (nZVI) and dioxygen ( $O_2$ ) has recently been demonstrated to chemically destroy a variety of organic species via oxidation. The degradation of these organic pollutants may be attributed to reactive oxygen species (ROS) production. This study is to enhance the ROS yield using bimetallic nZVI particles. ROS were measured under different species and contents of secondary metals and quantified by indirect probe compound tests. The ROS production was monitored over a pH range of 3-9 by measuring oxidation byproducts, formaldehyde (HCHO) and acetone. The results exhibit higher (HCHO) concentration levels, from the oxidation of methanol, for bimetallic nZVI than ZVI. At circumneutral pH, bimetallic nZVI with  $[Pd]/[Fe] = 5\%$ ,  $[Ni]/[Fe] = 10\%$  and  $[Ag]/[Fe] = 1\%$ , produced 22%, 93% and 87% higher HCHO concentration compared to nZVI, respectively, due probably to greater ROS production. The second metal additive increases significantly the ROS production, having an important effect on the mechanisms of ZVI-mediated oxidation.

## RESUMEN

Una nueva técnica de remediación que involucra la utilización de hierro de cero valencia a escala nano (nZVI) en presencia de dióxígeno ( $O_2$ ) ha sido investigada, demostrándose que puede destruir una gran variedad de contaminantes a través del proceso de oxidación. La degradación de contaminantes es llevada a cabo por la creación de especies reactivas oxidantes (ERO). El propósito de esta investigación es el incremento de estas especies oxidantes utilizando nanopartículas bimetálicas de hierro de cero valencia. Para poder analizar las ERO fue necesario crear diferentes tipos de nanopartículas bimetálicas y contenidos de segundos metales agregados a la superficie de las nanopartículas de hierro. La producción de ERO fue monitoreada en un rango de pH de 3 hasta 9. Como resultado, se observan niveles más altos de formaldehído (HCHO) en las nanopartículas bimetálicas donde las mismas con  $[Pd]/[Fe] = 5\%$ ,  $[Ni]/[Fe] = 10\%$  and  $[Ag]/[Fe] = 1\%$ , produjeron 22%, 93% y 87% más HCHO que las partículas no bimetálicas, teniendo un gran efecto en el incremento de las ERO.

Copyright © 2010 by Iván Morales Parra. All rights reserved. Printed in the United States of America. Except as permitted under the United States Copyright Act of 1976, no part of this publication may be reproduced or distributed in any form or by any means, or stored in a data base or retrieved system, without the prior written permission of the publisher.

## ACKNOWLEDGMENTS

First, I want to thank God, who has given me the strength and health to achieve this goal; my advisor Dr. Sangchul Hwang, for his farseeing guidance, endless support and generous help throughout this research. Also, thanks to my faculty committee members: Dr. Yang Deng and Dr. Jorge Rivera Santos for their cooperation. Special thanks to Dr. Wei-xian Zhang in the Department of Civil and Environmental Engineering at Lehigh University for his advice.

Thanks to Puerto Rico NSF-EPSCoR/RII Institute of Functional Nanomaterials through the New Faculty Start-Up Award for the financial support and the Department of Civil Engineering and Surveying at the University of Puerto Rico at Mayagüez and Environmental Engineering Laboratory, especially to Perla Torres who did whatever it took to keep everything working.

I would like to thank all my friends: Francisco Cruz, Gerson Ardila, Víctor de La Cruz, Gabriel Uribe, Nelson Anaya, Yasson Duque, Carolina Delgado, Ixia Aviles, Andrés Morales, Edwin de La Cruz, Andrea Gabanzo, Fernando Pantoja, María del Pilar Sierra, Omar Báez, and my lab partners: María de Lourdes Irrizarry, Julieta Gómez, Daniel Concepción, Edualberto Rosario, Marietta Marcano, Margarita Otero, Juan Carlos Falcón, Isomar Latorre, Ángel Anaya, and Zalleris Escobar. Also, I want to thank Federico García and Sylvia Abudo, for their true friendship and support.

I am very grateful to my father Jose Morales, for their financial support. To my beloved mother Mireya Parra, for always taking care of me and what I'm today. My brother and sister, Runny and Rosmery. I want to thank my beloved wife Dinelys and my little girl Lia Marie, for believe in me and try to do all these days easier. I dedicate this thesis to both of you.

## TABLE OF CONTENTS

1. INTRODUCTION.....	1
1.1 JUSTIFICATION.....	2
1.2 OBJECTIVES.....	3
2 LITERATURE REVIEW.....	4
2.1 GROUNDWATER AND SOIL CONTAMINATION.....	4
2.1.1 Introduction.....	4
2.1.2 Source of Groundwater Contamination.....	5
2.1.3 Types of Contaminants.....	6
2.1.4 Groundwater Quality Protection.....	9
2.1.5 Superfund and Comprehensive Environmental Response, Compensation, and Liability Act (CERCLA).....	9
2.1.6 Resource Conservation and Recovery Act (RCRA).....	13
2.2 ENVIRONMENTAL REMEDIATION TECHNIQUES.....	14
2.2.1 Soil Vapor Extraction.....	15
2.2.2 Air Sparging.....	15
2.2.3 In-Situ Chemical Oxidation.....	16
2.2.4 Fracturing.....	17
2.2.5 in Situ Flushing.....	17
2.2.6 In Situ Thermal Treatment Methods.....	17
2.2.7 Monitored Natural Attenuation.....	18
2.2.8 Permeable Reactive Barriers.....	19
2.2.9 Phytoremediation.....	19
2.2.10 Soil Washing.....	20
2.2.11 Solvent Extraction.....	21
2.3 ZVI AND NZVI-BASED REDUCTION FOR REMEDIATION.....	21
2.4 ZVI-BASED OXIDATION PROCESS (ZVI/O <sub>2</sub> ).....	26
2.4.1 Introduction.....	26

2.4.2 ROS Formation in ZVI/O <sub>2</sub> System .....	27
2.4.3 Degradation of Contaminants via Oxidation.....	29
2.5 METHODS FOR nZVI NANOPARTICLES SYNTHESIS .....	30
2.6 CHARACTERIZATION OF nZVI NANOPARTICLES .....	32
2.6.1 nZVI Core-shell Structure.....	32
2.6.2 Specific Surface Area .....	33
3. MATERIALS AND METHOD .....	35
3.1 Chemicals.....	35
3.2 Synthesis of nZVI and bimetallic nZVI.....	35
3.3 Morphology of nZVI particles .....	37
3.4 Batch Experiments .....	39
3.5 Quantification of Reactive Oxidant Species (ROS) .....	40
3.5.1 2,4-dinitrophenylhydrazine (DNPH) Derivatization of Aldehydes and Ketones.....	40
3.5.2 Separation of Aldehyde and Ketone Hydrazone by High performance Liquid chromatography (HPLC) and UV detection .....	41
3.6 Measurement of Hydrogen Peroxide (H <sub>2</sub> O <sub>2</sub> ) and Ferrous Iron (Fe <sup>2+</sup> ) .....	43
4. RESULTS .....	46
4.1 Characterization of Nanoparticles .....	46
4.2 Quantification of HCHO.....	48
4.2.1 Effects of Secondary Metal Content and Solution pH in The Overall HCHO Production.....	49
4.2.2 Effects of Secondary Metal Content and Solution pH in Hydroxyl Radicals .....	53
4.3 Track of the Key Intermediates.....	56
4.3.1 Production of Ferrous Ion (Fe <sup>2+</sup> ) .....	56
4.3.2 Production of Hydrogen Peroxide (H <sub>2</sub> O <sub>2</sub> ).....	58
5. DISCUSSION.....	61
5.1 ROS production at different pH .....	61
5.2 Nature and Identity of ROS .....	63
6. CONCLUSIONS AND RECOMENDATIONS.....	64
7. REFERENCES .....	66

## LIST OF TABLES

Table 1 Contaminant source and location in groundwater .....	5
Table 2 Superfund sites around United States .....	10
Table 3 Puerto Rico superfund sites in NPL, location and Contaminant type found. Source: EPA.....	12
Table 4 RCRA site list in Puerto Rico.....	13
Table 5 Chemical oxidation technologies (Yin and Allen, 1999).....	16
Table 6 Optimal PH for compounds degradation by ZVI .....	23
Table 7 Environmental Contaminants reduced by nanoscale zero iron valent. ....	25
Table 8 Methods for nanoparticles synthesis.....	31
Table 9 BET surface area and shapes for different samples. Source: Liu, 2005. ....	34
Table 10 secondary metal content and dilution factor for bimetallic nZVI.....	37

## LIST OF FIGURES

Figure 1 Puerto Rico superfund Sites with cleanup construction completed and deleted from NPL.....	11
Figure 2 Reaction mechanisms in ZVI-based reduction of contaminants. Source: Matheson & Tratnyek (1994).....	22
Figure 3 Application of nZVI for in situ remediation. Source: Zhang (2003) .....	24
Figure 4 Proposed primary reaction pathways in ZVI-mediated oxidation (Circle symbols indicate key intermediates; and square symbols indicate the reactants. Fe(II) and Fe(III) represent total free, hydrolyzed and complexed ferrous and ferric species, respectively). ...	28
Figure 5 nZVI core-shell structure and the conceptual reaction diagram of nZVI/O <sub>2</sub> system. Particle size and shell thickness ranges around 20-40 nm and 2-3 nm (Li, 2005; Liu, 2005; Nurmi, 2005), respectively .....	32
Figure 6 nZVI particles suspension.....	36
Figure 7 Scanning Electron Microscope (SEM) .....	38
Figure 8 Serum vials filled with O <sub>2</sub> -saturated pH buffered solutions.....	39
Figure 9 Vials in a water bath shaker .....	39
Figure 10 Reaction Mechanism between 2,4 DNPH and aldehyde or ketone. Source: Shriner et al., (2004) .....	41
Figure 11 HCHO calibration curve .....	42
Figure 12 C <sub>3</sub> H <sub>6</sub> O Calibration curve .....	43
Figure 13 Ferrous Calibration Curve.....	44
Figure 14 Hydrogen Peroxide Calibration Curve .....	45
Figure 15 SEM images of iron nanoparticles at a) 10000X and b) 9000X magnification ....	46
Figure 16 SEM images of iron nanoparticles at a) 20000X and b) 35000X magnification ..	47
Figure 17 Production of HCHO from [Ni]/[Fe]= 0.10, [Pd]/[Fe] = 0.05, [Ag]/[Fe] = 0.01 over time. CH <sub>3</sub> OH Initial Concentration = 195 μM; [Fe <sub>0</sub> ] = 400 μM; pH = 6.....	48
Figure 18 Production of HCHO from [Pd]/[Fe]= 0.01, [Pd]/[Fe] = 0.05, [Pd]/[Fe] = 0.10. CH <sub>3</sub> OH Initial Concentration = 195 μM; [Fe <sub>0</sub> ] = 400 μM; Reaction Time = 180 min .....	50
Figure 19 Production of HCHO from [Ni]/[Fe]= 0.01, [Ni]/[Fe] = 0.05, [Pd]/[Ni] = 0.10. CH <sub>3</sub> OH Initial Concentration = 195 μM; [Fe <sub>0</sub> ] = 400 μM; Reaction Time = 180 min .....	51
Figure 20 Production of HCHO from [Ag]/[Fe] = 0.01, [Ag]/[Fe] = 0.05, [Ag]/[Ni] = 0.10. CH <sub>3</sub> OH Initial Concentration = 195 μM; [Fe <sub>0</sub> ] = 400 μM; Reaction Time = 180 min .....	52

Figure 21 Comparison of the maximum HCHO production at different pH and secondary metal contents.....	53
Figure 22 Production of C <sub>3</sub> H <sub>6</sub> O from [Pd]/[Fe]= 0.01, [Pd]/[Fe] = 0.05, [Pd]/[Fe] = 0.10. 2-Propanol Initial Concentration = 250 μM; [Fe <sub>0</sub> ] = 400 μM; Reaction Time = 180 min .....	54
Figure 23 Production of C <sub>3</sub> H <sub>6</sub> O from [Ni]/[Fe]= 0.01, [Ni]/[Fe] = 0.05, [Ni]/[Fe] = 0.10. 2-Propanol Initial Concentration = 250 μM; [Fe <sub>0</sub> ] = 400 μM; Reaction Time = 180 min .....	55
Figure 24 Production of C <sub>3</sub> H <sub>6</sub> O from [Ag]/[Fe]= 0.01, [Ag]/[Fe] = 0.05, [Ag]/[Fe] = 0.10. 2-Propanol Initial Concentration = 250 μM; [Fe <sub>0</sub> ] = 400 μM; Reaction Time = 180 min ...	56
Figure 25 Production of Ferrous Iron from [Ni]/[Fe]= 0.10, [Pd]/[Fe] = 0.05, [Ag]/[Fe] = 0.01 over time. [Fe <sub>0</sub> ] = 400 μM; pH = 4. ....	57
Figure 26 Production of Ferrous Iron from [Ni]/[Fe]= 0.10, [Pd]/[Fe] = 0.05, [Ag]/[Fe] = 0.01 over time. [Fe <sub>0</sub> ] = 400 μM; pH = 6 .....	58
Figure 27 Production of hydrogen peroxide from [Ni]/[Fe]= 0.10, [Pd]/[Fe] = 0.05, [Ag]/[Fe] = 0.01 over time. [Fe <sub>0</sub> ] = 400 μM; pH = 4 .....	59
Figure 28 Production of Hydrogen Peroxide from [Ni]/[Fe]= 0.10, [Pd]/[Fe] = 0.05, [Ag]/[Fe] = 0.01 over time. [Fe <sub>0</sub> ] = 400 μM; pH = 6 .....	60

# 1. INTRODUCTION

Contamination of groundwater and soil caused by the improper handling of toxic substances or the leakage of toxic chemicals from storage containers poses serious environmental concerns. For example, in Puerto Rico, 18 Superfund sites are located within 14 municipalities, of which most were contaminated by landfill leakage, pesticide usage, and pharmaceutical waste discharge (EPA, 2009). Traditional remediation methods (e.g. pump-and-treat process) may be extremely costly and time-taking. Reliable and cost-effective innovative remediation alternatives are highly needed to shorten the time for site closure and accelerate the cleanup.

A new remediating process involving zero-valent iron (ZVI) and dioxygen ( $O_2$ ) has recently been demonstrated to chemically destroy a variety of organic species such as herbicides (Joo et al., 2004 and 2005) and chelating agents ( Noradoun & Cheng, 2005; Englehardt et al., 2007) via oxidation, mechanistically different from ZVI-based dechlorination via reduction. However, more than 95% of ZVI is typically corroded rather than utilized for production of the reactive oxygen species (ROS) in the ZVI/ $O_2$  system. Consequently, this process cannot be applied into practice.

The proposed study presents research designed to evaluate the feasibility of using bimetallic nanoparticulate ZVI (nZVI) to enhance the ROS yield, and elucidate key mechanisms in the oxidation improvement. By replacing common ZVI particles by bimetallic nZVI, the ROS yield enhancement may result due to formation of a galvanic cell between the two metals, leading to more electron transfer.

## 1.1 JUSTIFICATION

ZVI has been applied as part of remediation techniques for the degradation of a variety of contaminants, present in groundwater and soil, due to human activities. Its application started in the early 1990's with the construction of permeable reactive barriers (PRB). Costs and flexibility, related to the structure construction and location, derived in an unfeasible use for PRB's. In the process, ZVI is used under anaerobic conditions where ZVI can reduce chlorinated organic compounds (e.g. TCE), and the produced iron corrosion products can absorb toxic inorganic species such as arsenic. However, high operational costs associated with the structure construction, as well as the limitation in the treatment depth, has prevented application of the PRB technology in many sites.

Since the late 1990s, in-situ injection of nanoscale zero-valent iron (nZVI) has become an alternate for conventional ZVI PRB. nZVI particles are expected to freely move in the subsurface environment and access a very deep contaminant site. Moreover, nZVI possesses much greater specific surface area and faster reaction kinetics, which allow the higher efficiency in degradation of organic compounds.

In the past few years, an innovative oxidative process based on ZVI has been studied. It has been demonstrated that ZVI oxidizes organic compounds in presence of oxygen (ZVI/O<sub>2</sub>), such as chlorinated phenols and herbicides (Noradoun et al., 2003 and Joo et al., 2004). However, ZVI/O<sub>2</sub> has been limited by the following barriers: (1) decrease of iron reactivity over time, probably due to the formation of surface passivation layers or due to the precipitation of metal hydroxides [e.g., Fe(OH)<sub>2</sub>, Fe(OH)<sub>3</sub>] and metal carbonates (e.g., FeCO<sub>3</sub>) on the surface of iron; and (2) the production level of reactive oxidative species (ROS) is very low compared with the iron quantity used (more than 95% of ZVI is typically corroded rather than utilized).

The first main concern has been partially overcome by addition of a chelating agent (e.g., EDTA). This chelating agent prevents passivation by reducing the presence of accumulated Fe<sup>2+</sup> near the surface and therefore decreases the blocking of passivation layers on the reactions between ZVI and oxygen. Use of a chelating agent is affected by such factors as pH, the ratio of EDTA to Fe, and the O<sub>2</sub> level (Keenan & Sedlak, 2008).

However, for the second concern, there is not an effective method to significantly increase the ROS level. This study was designed to evaluate the feasibility of using bimetallic nZVI to enhance the ROS yield, and elucidate key mechanisms in the oxidation improvement.

## **1.2 OBJECTIVES**

The overall objective of this proposed study is to maximize the potential of activating molecular oxygen in the ZVI/O<sub>2</sub> system using bimetallic nanoparticulate ZVI for remediation of organic compound-contaminated groundwater and soil. By replacing common nZVI particles with bimetallic nZVI particles, new and unexpected phenomena may result due to formation of a galvanic cell between the two metals to enhance the electron transfer. The central hypothesis is that the ROS yield will be significantly increased to improve the oxidation efficiency when the bare nZVI is replaced with the bimetallic nZVI.

Specific objectives of this research are to:

- (1) Synthesize and characterize nZVI and bimetallic nZVI particles;
- (2) Determine the ROS yield, and identify the ROS species (hydroxyl radicals or ferryl) for different bimetallic nZVI at different reaction conditions;
- (3) Determine the most favorable metal additive and its optimal content to enhance the oxidation in the nZVI/O<sub>2</sub> system; and
- (4) Track the concentrations of important intermediates to better understand the oxidative mechanism.

## **2 LITERATURE REVIEW**

### **2.1 GROUNDWATER AND SOIL CONTAMINATION**

#### **2.1.1 Introduction**

Groundwater represents an important water source to support human activities in the United States, particularly for production of drinking water. However, groundwater has been widely contaminated by a variety of contaminants.

The U.S. Geological Survey (USGS) reported that ground-water use increased from about 35 billion gallons per day in 1950 to about 83 billion gallons per day in 2005, which means that one-fifth of all fresh water used in the United States in 2005 derived originally from groundwater. Groundwater supplied through a public water supply system or from a private well, provides approximately 33 percent of the public water supply for urban and rural areas, meeting with water needs of more than 258 million US people.

In general, more than 40% of the water used for agricultural purposes is drawn from groundwater (Kenny et al., 2009). Many states, such as Nebraska, Arkansas, Texas, Kansas, Mississippi, and Missouri, use more than 90 percent of their ground-water withdrawals for agricultural activities. Approximately, two-thirds of the fresh groundwater withdrawals in 2005 were for irrigation, and more than one-half of the groundwater for irrigation was withdrawn in just four States: California, Nebraska, Arkansas, and Texas. In addition, approximately 21 percent of all ground water is used for industrial purposes.

In Puerto Rico, about 722 MGD (million gallons per day) of fresh and saline water were withdrawn from all water sources in 2005. Of this total about 20.4% or 147 MGD were groundwater withdrawals. Puerto Rico has three important aquifer systems: alluvial valley aquifers, the South Coast aquifer, and the North Coast Limestone aquifer system (Veve & Taggart, 1996). In 1985, these aquifer systems supplied 17%, 42% and 38.8% of total groundwater withdrawals for public supply, industrial and agricultural use, respectively (Miller et al., 1997).

### 2.1.2 Source of Groundwater Contamination

Ground-water contamination can occur on the ground surface, in the vadose zone, or in the saturated zone. Various activities can cause different groundwater contamination in different depths (Table 1). Where a contaminant originates is a factor that can affect its impacts on ground-water quality. For example, if a contaminant is spilled on the ground surface or injected into the vadose zone, it may have to move through several layers of soil with different properties before it reaches the ground water. As the contaminant moves through these layers, various physical, chemical, biological processes occur to minimize the final effect of the contaminant in ground water.

In addition, the efficiencies of these processes are affected by the transport pathway distance between the ground water and contaminant source and the time needed to reach the ground water. If the contaminant is introduced directly into saturated zone, the primary process that can influence the effect of the contaminant is dilution by the surrounding ground water.

Due to the slow movement of groundwater, once a contaminant reaches the ground water, little dilution or dispersion normally occurs. The contaminant forms a concentrated plume that can flow along the same path as the ground water. Among the factors affecting the size, form, and rate of movement of the contaminant plume are the concentration and type of contaminant as well as the groundwater speed movement.

**Table 1 Contaminant source and location in groundwater**

Location	Ground surface	Vadose zone	Saturated Zone
Contaminant Source	Infiltration of polluted surface water	Septic tanks	Waste disposal in wells
	Land disposal of wastes	Ponds	Drainage wells
	Dumps	Sanitary landfills	Underground storage
	Sewage sludge disposal	waste disposal in excavations	Mines
	Animal feedlots	Underground storage tank leaks	Groundwater withdrawals
	Fertilizers & pesticides	Artificial recharge	Water supply wells
	Accidental spills		
	Airborne source particulates		

### 2.1.3 Types of Contaminants

Subsurface chemical pollutants can be derived naturally or produced by anthropogenic activities. Naturally occurring chemicals are mostly from minerals, such as iron, calcium, and selenium. Substances resulting from anthropogenic activities include synthetic organic chemicals and hydrocarbons (e.g., solvents, pesticides, and petroleum products); landfill leachates (liquids that have dripped through the landfill and carry dissolved substances from the waste materials), containing ammonia nitrogen, heavy metals, and refractory organics; heavy metals; salt; bacteria; and viruses.

EPA (2010d) has listed contaminants commonly found in the US contaminated sites (e.g., National Priority List sites) where they have applied remedial design. This list includes the following contaminants:

**Arsenic:** arsenic is a steel gray metal-like material. As an inorganic compound, arsenic can be found in copper or lead-containing minerals (EPA, 2010d). In groundwater, its presence is attributed to dissolved minerals from weathered rocks and soils. In United States, much arsenic is imported and used as a preservative for treated wood. Also, it can be found in lead-acid batteries, light-emitting diodes, paints, dyes, metals, pharmaceuticals, pesticides, herbicides, soaps, and semiconductors.

Long-term exposure of inorganic arsenic can cause the human death (>60 ppm). At a low dose, arsenic may cause irritation of the stomach and intestines, with symptoms such as stomach ache, nausea, vomiting, and diarrhea. Other effects might include decreased production of red and white blood cells, which can lead to fatigue, abnormal heart rhythm and blood-vessel damage.

**Chromium VI:** Cr can be found naturally in rocks, soil, plants, and animals. It occurs in combination with other elements as chromium salts, some of which are soluble in water (EPA, 2010d). Also chromium is used for steel manufacturing to avoid corrosion. In air, chromium can exist in the form of as particles. The concentration of naturally occurring chromium in U.S. soils ranges from 1 to 2,000 parts per million.

In nature, it can be found as hexavalent chromium and trivalent chromium. Hexavalent chromium is known as human carcinogen due to chronic inhalation exposures. When swallowed, it can damage the liver and kidneys

**Dense Non-aqueous Phase Liquids (DNAPLs):** DNAPLs are slightly soluble compounds or mixtures of chemicals heavier than groundwater (EPA, 2010d). Over 70 DNAPLs or mixtures were identified (Cohen & Mercer, 1993). Most of them are solvents and feedstock. According to EPA, the major DNAPLs found in superfund sites are:

- Ethers
- Halogenated alkanes
- Halogenated alkenes (1,1-Dichloroethene, cis 1,2-Dichloroethene, trans 1,2-Dichloroethene, cis 1,3-Dichloropropene, trans 1,3-Dichloropropene, Tetrachloroethene, Trichloroethene, Halogenated monaromatics, Polychlorinated biphenyls (PCBs))
- Multi-Component Waste (Coal Tars, Creosotes, Heavy Oils)
- Other (aniline, benzyl chloride, etc.)

These compounds typically cause damage to kidney, liver, nervous system, and some of them are carcinogenic.

**1,4-Dioxane (C<sub>4</sub>H<sub>8</sub>O<sub>2</sub>):** 1,4-dioxane is mostly used for industrial purposes, as solvent in paints, lacquers, cosmetics, deodorants, etc (EPA, 2010d). Frequently, 1,4-dioxane is used together with chlorinated solvents, particularly 1,1,1-trichloroethane (TCA), as a stabilizer and corrosion inhibitor. EPA has considered 1,4-dioxane a potential human carcinogen based on the results of animal studies.

**Dioxins:** dioxins are produced commercially only for toxicological and chemical research. Their appearance into the environment has been accidental due to chemical reactions involving chlorine and various combustion processes that produce undesirable and uncontrolled byproducts (EPA, 2010d). Before they were banned, a major source of dioxins was in the manufacture and application of phenoxy herbicides, which could contain 2,3,7,8-TCDD at the level of parts per million (ppm). Dioxins such as polychlorinated dibenzodioxins (PCDDs) may

cause changes in metabolism as well as estrogen metabolism, deriving in thyroid stimulation and subsequent thyroid and liver cancer.

**Mercury (Hg):** The most common natural forms of mercury found in the environment are metallic mercury, mercuric sulfide, mercuric chloride, and methylmercury (EPA, 2010d). Mercury and its compounds have a great presence in industrial, medicinal, cosmetic, and spiritual uses. Modern uses for mercury include electrical switches, thermometers and dental amalgams. Elemental mercury may cause tremors, gingivitis, and excitability, and even death at high levels of exposure. Elemental mercury slow digestion may pass through the digestive system without causing damage.

**Methyl Tertiary Butyl Ether (MTBE):** MTBE was a chemical compound used as gasoline additive to reduce harmful air emissions. However, its use has caused serious wide spreading and contamination in drinking water (EPA, 2010d). MTBE inhalation in high concentrations may cause cancer.

MTBE is a very difficult chemical to remediate. Compared to other gasoline organic components, its removal from drinking water is very expensive because some low-cost cleanup technologies cannot be applied (e.g., bioremediation) due to its stable chemical structure.

**Perchlorate:** perchlorate may occur in natural environment or produced through anthropogenic activities. Its presence is associated with use of ammonium, potassium, and sodium perchlorate salts (EPA, 2010d). Perchlorate is highly mobile in surface and subsurface aqueous systems. This toxic chemical can exist in water for a long period of time due to inert characteristic under typical groundwater conditions.

Perchlorate can inhibit the iodine uptake of thyroid, disrupt thyroid functions and cause important effect in metabolism. The disruption of thyroid functions in pregnant mothers can directly affect the fetus. Its negative effects include changes in behavior, delayed development and decreased learning capability.

**Trichloroethylene (TCE):** TCE is used as a solvent in automotive and metal machinery industry. It can be found as component in paint removers, adhesives and spot removers (EPA, 2010d). Previously, TCE was used in foods and beverages (decaffeination of coffee), pharmaceuticals and cosmetics. Usually, this chemical cannot occur naturally in the environment.

Chronic exposure has been associated with liver damage, kidney and nervous system. At high vapor concentrations, TCE may cause respiratory tract irritation. Long term exposure may lead to unconsciousness.

#### **2.1.4 Groundwater Quality Protection**

The groundwater quality is monitored by U.S. Environmental Protection Agency. This activity is supported by several federal laws such as (EPA, 1990):

- Safe Drinking Water Act
- Comprehensive Environmental Response, Compensation, and Liability Act (CERCLA) (Superfund)
- Federal Insecticide, Fungicide, and Rodenticide Act
- Toxic Substances Control Act
- Clean Water Act
- Resource Conservation and Recovery Act (RCRA)

The implementation of these laws ensures the prevention of the supplies of groundwater from contamination, as well as saves time and money in cleanup technologies.

#### **2.1.5 Superfund and Comprehensive Environmental Response, Compensation, and Liability Act (CERCLA)**

CERCLA authorizes the government to clean all contaminated sites with hazardous waste or toxic chemicals caused by spills and that could be an environmental threat (EPA, 1990). This law was amended in 1986; this part authorizes citizen to sue polluters or law violators. CERCLA established an environmental program to address contaminated sites, which is called Superfund. The program assigns funds to assess and clean up contaminated sites.

EPA's Office of Solid Waste and Emergency Response (OSWER) in Washington, D.C. supervise the Superfund program. In this manner, EPA has 10 Regional offices around United States that administer Superfund program. For Superfund, EPA regions are the front line in responding to releases of hazardous substances and other emergencies. The regional offices manage more than 3,000 superfund sites (Table 2).

**Table 2 Superfund sites in United States**

<b>EPA Regional Office</b>	<b>State</b>	<b># Superfund sites</b>
1	ME NH VT MA RI CT	117
2	NY NJ PR VI	1277
3	PA DE DC MD VA WV	595
4	KY TN NC SC MS AL GA FL	265
5	MN WI IL MI IN OH	318
6	NM TX OK AR LA	131
7	NE KS IA MO	90
8	MT ND WY SD UT CO	69
9	CA NV AZ HI	148
10	WA OR ID AK	29

The superfund cleanup process involves several steps (EPA, 2010c):

- **Preliminary Assessment/Site Inspection:** investigates site conditions; if contamination needs urgent response actions or need to be placed in National Priority List.
- **National Priorities List (NPL) Site Listing Process:** list of the most serious sites identified for possible long-term cleanup. In Puerto Rico, there are 19 Superfund sites distributed in 14 municipalities. The contamination source was identified such as landfill leakage, pesticide usage, and pharmaceutical waste discharge (**Table 3**).
- **Remedial Investigation/Feasibility Study:** evaluates extent of contamination and application of treatment technology and cost.
- **Records of Decision:** elucidate the cleanup alternatives that will be used in the NPL sites.
- **Remedial Design/Remedial Action:** preparation and implementation of plans and specifications for applying site remedies.

- **Construction Completion:** notifies completion of physical cleanup construction. In Puerto Rico, 14 sites have been completed.
- **Post Construction Completion:** ensures that response actions provide for the long-term protection of human health and the environment.
- **National Priorities List Deletion:** removes a site from NPL, since all cleanup goals are accomplished. In Puerto Rico, only 5 superfund sites have been deleted from NPL.
- **Site Reuse/Redevelopment:** use of the hazardous waste sites without affecting the remedy.



**Figure 1 Puerto Rico superfund Sites with cleanup construction completed and deleted from NPL.**

**Table 3 Puerto Rico superfund sites in NPL, location and Contaminant type found. Source: EPA**

Site Name	Municipality	Contaminant Type
Atlantic Fleet Weapons Training Area	Vieques	Mercury, lead, copper, magnesium, lithium, perchlorate, TNT, napalm, and depleted uranium
Barceloneta Landfill	Florida	Heavy metals and volatile organic compounds (VOCs)
Cidra Groundwater Contamination Site	Cidra	Volatile organic compounds (VOCs)
Fibers Public Supply Wells	Guayama	Volatile organic compounds (VOCs)
Frontera Creek	Humacao	Mercury (sediments and soil)
GE Wiring Devices	Juana Diaz	Mercury, volatile organic compounds (VOCs)
Juncos Landfill	Juncos	Heavy metals and chloroform
Maunabo Area Ground Water Contamination Site	Maunabo	Chlorinated solvents (PCE, TCE, DCE)
Naval Security Group Activity	Toa Baja	Heavy metals, pesticides, Polychlorinated byphenyls
Papelera Puertorriqueña Inc.	Utua	Benzene, toluene, tetrachloroethylene (PCE), ethyl benzene, and trichloroethylene (TCE)
Pesticide Warehouse I (PWI)	Arecibo	Pesticides, including aldrin, endrin, endrin aldehyde, gamma-chlordane, toxaphene, diazinon, and diuron
RCA Del Caribe	Barceloneta	Ferric chloride
San Germán Ground Water Contamination Site	San Germán	Chlorinated solvents (PCE, TCE, DCE)
Scorpio Recycling, Inc. Site	Toa Baja	Lead, vanadium and barium
Upjohn Facility	Barceloneta	Carbon tetrachloride and its degradation products
V&M/Albaladejo	Vega Baja	Heavy metals, including antimony, cadmium, copper, silver and lead
Vega Baja Solid Waste Disposal Site	Vega Baja	Lead, arsenic, pesticides
Vega Alta Public Supply Wells	Vega Alta	Volatile organic compounds (VOCs)

### 2.1.6 Resource Conservation and Recovery Act (RCRA)

The Resource Conservation and Recovery Act controls the storage, transportation, treatment, and disposal of solid and hazardous wastes for prevention of contaminants from leaching into ground water from municipal landfills, underground storage tanks, and hazardous waste disposal facilities (EPA, 1990). The Resource Conservation and Recovery Act, Subtitle C, regulates facilities that generate, treat, store, or dispose of hazardous waste. RCRA subtitle C addresses two paths (EPA, 2010a):

1. Prevention of environmental problems by ensuring that wastes are well managed from "cradle to grave," reducing the amount of waste generated, conserving energy and natural resources, and
2. Cleaning up environmental problems caused by the mismanagement of wastes.

EPA administers 17 Puerto Rico sites under RCRA. These sites are located in 15 municipalities.

**Table 4 RCRA site list in Puerto Rico**

Site Name	Municipality
Boricua Wood Processing, Inc.	Toja Baja
Bristol-Myers Squibb Manufacturing Company	Humacao
Caribbean Petroleum Refining, L.P.	Bayamon
Caribe General Electric Products, Inc. Juana Diaz	Juana Diaz
Chevron Phillips Chemical Puerto Rico Core	Juana Diaz
Commonwealth Oil And Refining Company, Inc.	Guayama
Compaq Computer Corporation	Sabana Grande
GE Puerto Rico Investment, Inc..	Patillas
GE Residential Products, Inc.	Rio Grande
Merck, Sharp & Dohme Quimica de Puerto Rico	Barceloneta
Naval Activity Puerto Rico	Ceiba
Omark Caribbean Incorporated	Bayamon
Pharmacia & Upjohn Caribe, Inc.	Arecibo
PPG Discontinued Operations Site	Guayanilla
Shell Chemical Yabucoa Incorporated	Yabucoa
TAPI Puerto Rico, Inc.	Guayama
Union Carbide Caribe, LLC , UCCLLC	Peñuelas

## 2.2 ENVIRONMENTAL REMEDIATION TECHNIQUES

Remediation is a cleanup of a contaminated environmental site (e.g. soil and groundwater) to a condition that cannot affect the human health. Therefore, remediation means removal of harmful chemicals from these sites or transform of them into benign species.

State and federal governments have instated several environmental regulations to preserve the groundwater quality and restore contaminated sites from a variety of contaminants. In this manner, the Environmental Protection Agency (EPA) has created a list of superfund sites that are considered for remedial action, this is called the Comprehensive Environmental Response, Compensation, and Liability Information System (CERCLIS). All superfund sites included in this inventory are ready for remedial action.

For remedial action, a number of aspects have to be taken into consideration, such as:

- Contaminant identification and extent.
- Type of treatment to be applied.
- Meet the Maximum Contaminant Level (MCL) for the site to be treated.

EPA uses different methods to clean up superfund and other contaminated sites. Most of these technologies are alternatives for traditional cleanup methods, emerging from the 1990's, because conventional methods used were inappropriate to remediate the polluted sites. A typical traditional method is to excavate contaminated soil and transport it to landfills. However, the transportation cost is usually and toxic chemicals remain untreated. In another traditional process, the so-called pump-and-treat, contaminated groundwater was removed from subsurface, subsequently treated above the ground, and re-injected back to aquifers. However, the process could take a few decades until treatment is completed, and the additional cost associated with such a long treatment may also cause the cleanup infeasible in cost.

Removal of contaminants through the pump and treat technology depends extremely on the contaminant nature and the subsurface geology. This technology is applicable to contaminated sites where the chemicals are mobile, and media sorption is negligible (Nyer, 1993). Another factor that can affect pump and treat technique is the heterogeneity of the subsurface

hydrogeology. Pump and treat is not appropriate to contaminants with high residual saturation (contaminants tend to be sorbed in the soil), contaminants with high sorption capabilities and homogeneous aquifers with hydraulic conductivity less than  $10^{-5}$  cm/sec (FRTR, 2010). The biofouling of extraction wells and treatment stream derived from this issue also limit the performance of this technology.

The main advantages of innovative cleanup methods are shorter cleanup time and lower cost, compared with conventional methods. A short description of the most frequently used remediation alternatives is as follows.

### **2.2.1 Soil Vapor Extraction**

Soil vapor extraction (SVE) is an in situ unsaturated (vadose) zone soil remediation technology in which a vacuum pumps a flow of air into the contaminated vadose zone and strip out volatile and some semivolatile organic compounds (EPA, 2010b). Then, the removed gas from the soil is collected and treated above the ground

This technology is applicable for VOCs and some fuels with Henry's law constant greater than 0.01. The treatment efficiency is affected by the moisture content, organic content, and air permeability of the soil. SVE is limited in soil with high percentage of fines and degree of saturation.

### **2.2.2 Air Sparging**

Air sparging involves the injection of air through a contaminated aquifer. Injected air passes through the soil pores in all directions, causing the volatile organic compounds removal by volatilization (Miller R. , 1996). As a result, the contaminants are flushed into the unsaturated zone. This process produces vapor-phase contamination in the soil vadose zone. In addition, SVE is utilized with air sparging to remove this contamination. Removal times are extremely shortened compared with other technologies, and cost is less combined with SVE. Moreover, air sparging is limited by hydrogeologic settings. It cannot be used for treatment of confined aquifers and is not recommended in stratified soils.

### 2.2.3 In-Situ Chemical Oxidation

In situ chemical oxidation (ISCO) technology is the cleanup of pollution in soil and groundwater through reduction-oxidation (redox) reactions caused by the externally added strong oxidizing agents. This method has a great potential to transform a broad range of contaminants (e.g. hydrocarbons) into harmless chemicals, such as water and carbon dioxide (Yin & Allen, 1999). This transformation can be attributed to the exchange of electrons between the oxidants and contaminants.

ISCO methods can be applied under different environmental conditions including saturated zones and capillary fringe (Huling & Pivetz, 2006). The most commonly used oxidizing agents are: a) potassium permanganate ( $KMnO_4$ ), hydrogen peroxide ( $H_2O_2$ ), and ozone ( $O_3$ ). A brief summary of these technologies is described in Table 5.

**Table 5 Chemical oxidation technologies (Yin and Allen, 1999).**

Technology	Target Compound	pH	Permeability	Temperature	Oxidant degradation
Permanganate	Chlorinated solvents, polynuclear aromatic hydrocarbons (PAHs), phenolics (including creosols), and cyanides	(7-8)	high	Ambient	can be easily degraded in soil and groundwater
Hydrogen Peroxide	Chlorinated solvents (TCE, PCE), Munitions (TNT, RDX), Pesticides (chlorophenoxy, atrazine, pendimethalin), Petroleum residues (BTEX, PAH, TPH, MTBE, diesel fuel), Wood preservatives (PCP, creosote), PCBs and phenolics	(2-4)	high	Ambient	stable
Ozone	aromatic hydrocarbons, pesticides, chlorinated solvents, and ordnance compounds	soil pH	high	Ambient	limited in soils

#### **2.2.4 Fracturing**

Fracturing is not considered directly as a remediation method. Its purpose is to break up rock or a fine soil to allow other technologies to enhance its cleanup efficiency (EPA, 2010). The fractures made in this process generate a pathway in which the toxic chemicals can be extracted, removed or destroyed. Three ways of fracturing are generally used:

- Hydraulic fracturing: The water is pumped under pressure into holes drilled in the ground.
- Pneumatic fracturing: uses air to break up soil.
- Blast-enhanced fracturing: uses explosives to fracture rock.

#### **2.2.5 in Situ Flushing**

In situ flushing pumps an aqueous solution into a contaminated groundwater or soil followed by immediate extraction, treatment and reinjection. This aqueous solution can be injected into vadose and saturated zones (Roote, 1997). The solutions utilized in this method include surfactants, cosolvents, acids, bases, oxidants, chelants, solvents and water. The main purpose of the solution is to increase the solubility and mobility of the contaminants and flushing rate. In situ flushing can be used to degrade: non-aqueous phase liquids (NAPL), volatile Organic compounds (VOC), polychlorinated biphenyls (PCBs), and halogenated pesticides. Also, inorganic and radioactive contaminants are susceptible to this remediation method.

One of the advantages of using in situ flushing is no need to excavate the soil to be treated. In situ flushing can be costly and complicated to use if many wells have to be constructed, or the amount of added chemicals is too high. The removal efficiency of this technology depends on type of contaminants and soil.

#### **2.2.6 In Situ Thermal Treatment Methods**

In situ thermal treatments degrade or destroy contaminants by applying heat to the polluted soil or groundwater to volatilize organic chemicals or enhance their mobility and subsequent extraction (EPA, 2010b). The extraction is completed through wells that capture these chemicals. Thereafter, the contaminants are treated ex situ. Thermal methods are

appropriate to clean up contaminated sites with dense or light non-aqueous phase liquids (DNAPLs or LNAPLs). The most frequently used in situ thermal methods are:

**Hot air/steam injection:** steam or hot air is injected under the polluted area. The steam heats up the contaminated soil and then mobilizes, evaporates, and destroys the harmful chemicals.

**Hot water injection:** similar to steam injection except that hot water is injected to contaminated soil instead of steam.

**Electrical resistance heating:** an electric current is used underground through wells made of steel. The electric current heats up the water and volatilize hazardous chemicals.

**Radio frequency heating:** this process utilizes electromagnetic energy to heat the soil.

**Thermal conduction:** in this method, the heat is provided to the contaminated sites through steel wells or with a blanket that covers the ground surface.

Similar to in situ flushing method, in situ thermal methods allow soil to be treated without digging out that usually requires a high cost. However, the treatment time of this method is typically longer than other methods mentioned above.

### **2.2.7 Monitored Natural Attenuation**

This method utilizes natural processes to treat or attenuate pollution in soil and groundwater. Natural attenuation processes involves a variety of physical, chemical, or biological processes that, under optimal conditions, may reduce the mass, toxicity, mobility, volume, or concentration of contaminants in soil or groundwater (EPA, 2001a).

Natural attenuation can be attributed to four natural processes:

- Microbes present in soil and groundwater degrade some toxic chemicals into innocuous compounds, or even water and carbon dioxide (mineralization).
- Chemicals are immobilized due to adsorption to soil.

- Chemicals are diluted when mixed with clean water to reduce the concentration.
- Chemicals are evaporated.

### 2.2.8 Permeable Reactive Barriers

PRBs are a remediation method that cleans up groundwater flow as it passes through a permeable treatment medium under natural hydraulic gradients (EPA, 2001b). They have been applied successfully in many sites across the United States and Canada. The barriers are built with agents such as: ZVI, chelators (ligands selected for their specificity for a given metal), sorbents, and microbes.

PRBs are typically affected by several factors such as:

- Depth and width of barrier.
- Loss of reactive capacity.
- The barrier permeability can be decreased by chemical precipitation (metal salts) or biological activities.
- Costs.

### 2.2.9 Phytoremediation

Phytoremediation is to use vegetation to clean contaminated sites. Vegetation sequesters, extracts, or degrades toxic chemicals located in soils and groundwater. A variety of organic and inorganic contaminants can be treated by phytoremediation, (EPA, 2000), including petroleum hydrocarbons, gas condensates, crude oil, chlorinated compounds, pesticides, explosive compounds, salts, heavy metals, metalloids, and radioactive materials. Six mechanisms contribute to the phytotechnologies:

**Phytosequestration:** a mechanism that immobilizes contaminants, particularly metals, within the root zone.

**Rhizodegradation:** a plant-assisted bioremediation in that the root zone (rhizosphere) increases microbial activity, therefore enhances the degradation of organic contaminants into

benign chemicals (e.g. petroleum hydrocarbons, PAHs, pesticides, BTEX, chlorinated solvents, PCP, PCBs, and surfactants) in the soil.

**Phytohydraulics:** the ability of plants to capture and evaporate water off the plant and take up and transpire water through the plant.

**Phytoextraction:** the extraction of contaminants through plant roots, followed by accumulation in plant tissue. Plants harvesting is required periodically because some plants accumulate contaminants to cause recontamination of the soil or groundwater.

**Phytovolatilization:** the phytodegradation of the harmful chemicals and transpiration of the degradation products to the atmosphere.

The efficiency of phytoremediation technologies depends on hydrogeology, climate conditions, groundwater geochemistry, and concentration of contaminants and plants characteristics.

### **2.2.10 Soil Washing**

Soil washing is a treatment process where contaminants are removed from the soil by aqueous chemicals and recovered from solution on a solid substrate. Then the contaminants are treated using different chemical, thermal or biological processes) (EPA, 2001c).

After all contaminants are removed from the soil, the bulk fraction that remains can be:

- used in the remediated site as backfill or on another site as fill;
- and/or disposed

The backfilling utilization reduces the cleanup and disposing of contaminated material. However, this method is not cost-effective in silty or clayey soils, as well as soils whose contamination is not significantly high.

### **2.2.11 Solvent Extraction**

Solvent extraction is to use an organic solvent to separate organic contaminants from soil. The organic solvent is mixed with contaminated soil in an extraction unit (EPA, 2001d). The type of solvent depends on soil characteristics and contaminant to be treated. The extracted solution then passes through a separator, where the contaminants and extractant are separated from the soil. In case that any solvent still remains in the soil after treatment, the soil is heated until the solvent is evaporated. One of the most important advantages of this technology is in situ application, to reduce transportation costs.

### **2.3 ZVI AND NZVI-BASED REDUCTION FOR REMEDIATION**

ZVI plays an important role in environmental remediation over the last decades. Under anaerobic conditions, ZVI is an excellent reducing agent to degrade many organic compounds, particularly chlorinated solvents, to detoxify the pollutants in subsurface. Simultaneously, the iron corrosion products can immobilize numerous inorganic pollutants such as heavy metals. Iron powders, filings, and micro-scale iron particles can be used in PRBs.

Matheson & Tratnyek (1994) explained the mechanism for the contaminants reduction through ZVI which presumably occurs in the iron surface area. The process is completed in three possible reaction pathways (Figure 2): a) direct electron transfer (ET) for  $\text{Fe}^0$  to the adsorbed contaminant or chlorinated compound (RX) at the metal-water interface, resulting in dechlorination and production of  $\text{Fe}^{2+}$ . b)  $\text{Fe}^{2+}$  resulting from corrosion of  $\text{Fe}^0$  may also dechlorinate RX and produce  $\text{Fe}^{3+}$  and c)  $\text{H}_2$  produced from the anaerobic corrosion of  $\text{Fe}^{2+}$  might react with RX in the presence of a catalyst.

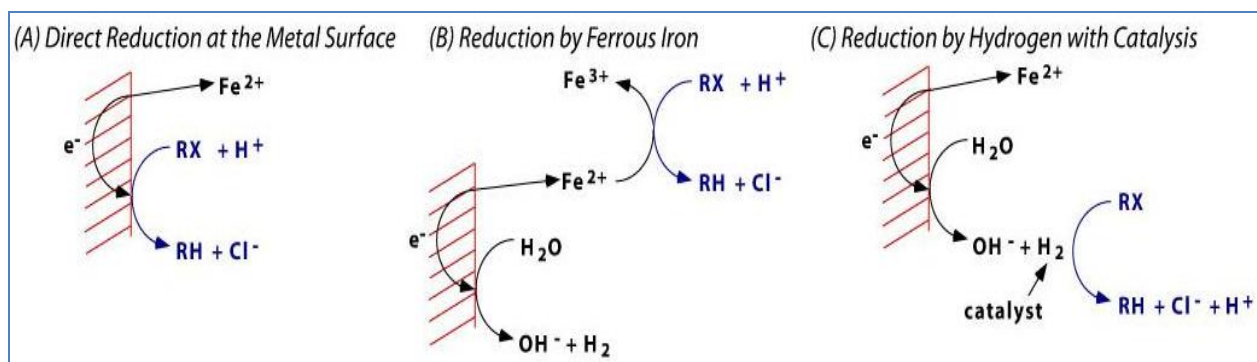


**Figure 2** Reaction mechanisms in ZVI-based reduction of contaminants. Source: Matheson & Tratnyek (1994)

This technology has been effective in the reduction of chlorinated pesticides (Sayles, 1997), chlorinated aromatics (Kim & Carraway, 2000) and halogenated organic compounds (HOC's) (Lu et al., 2004). The reduction of all these compounds exhibited an efficiency of 40% to 95%, including acceleration of transformation rates in 1 to 2 orders of magnitude.

The ZVI reductive capacity has been studied in the degradation of carbaryl, a pesticide used widely in agricultural activities. Carbaryl was rapidly reduced with a removal efficiency of 95% (Ghauch et al., 2001). The degradation of carbaryl is dependent on the amount of ZVI added.

Arsenic-contaminated groundwater remediation applying ZVI technology has been studied (Bang et al., 2005) (Sun et al., 2006). In the presence of oxygen, As(V) had more than 99.8% removal after 9 h, and As(III) showed 82.6% removal. When the solution was purged with nitrogen gas to remove dissolved oxygen (DO), less than 10% of the As(III) and As(V) was removed, attributing the removal efficiency to adsorption by iron hydroxides generated by oxidation of ZVI by O<sub>2</sub>. As reduction can be affected by the presence of phosphates and sulfates in aqueous solution, as well as humic acids (Sun et al., 2006). Table 6 shows the reported optimal conditions for different for compounds degraded by ZVI.

**Table 6 Optimal PH for compounds degradation by ZVI**

No.	pH	COMPOUNDS	ZVI Type	Time	Co ( $\mu$ M)	Removal Efficiency (%)	Final Products	Reference
1	6.6	Carbaryl	Iron Powder (325 Mesh)	40 min	199	95	--	Ghauch and Martin-Bouyer (2001)
2	7	DDT	Iron Powder	28800 min	8	93	--	Sayles et al. (1997)
3	7	Pentachlorophenol (PCP)	Electrolytic (100 Mesh) Bimetallic	840 min	37.5	50-80	Tetrachlorophenol (TeCP)	Kim and Carraway (2000)
4	7.4	Pentachlorophenol (PCP)	Iron Grains	840 min	37.5	99	Tetrachlorophenol (TeCP)	Kim and Carraway (2000)
5	7.5	Nitrobenzene	Granular Iron	40 min	80	92	--	Bell et al. (2003)
6	7.5	Trichloronitromethane (TCNM)	Electrolytic (100 Mesh)	40 min	100	99	--	Lee et al. (2007)
7	7.5	Trichloroacetonitrile (TCAN)	Electrolytic (100 Mesh)	40 min	100	99	--	Lee et al. (2007)
8	7.5	Trichloropropanone (1,1,1-TCP)	Electrolytic (100 Mesh)	160 min	45	99	--	Lee et al. (2007)
9	8	Hexachlorobenzene (HCB)	Iron Powder	1440 min	27.2	99	--	Lu et al. (2004)
10	8	TrichloroEthylene (TCE)	Iron Particles (100 Mesh)	1440 min	500	99	--	Chen et al. (2001)

In the 1990's, nanoscale zero valent iron (nZVI) and bimetallic nZVI were proposed for environmental remediation (Wang and Zhang, 1997). nZVI and palladized nZVI were synthesized exhibiting a smaller particle size (1 to 100 nm), larger specific surface area, and higher reactivity than iron filings and microsized iron powders. An unique advantage of nZVI is that it can be injected into the ground to reach the contaminated zone due to its fine size (<100 nm) (Nurmi et al., 2005; Li et al., 2006), so that the treatment occur in place (Figure 3).

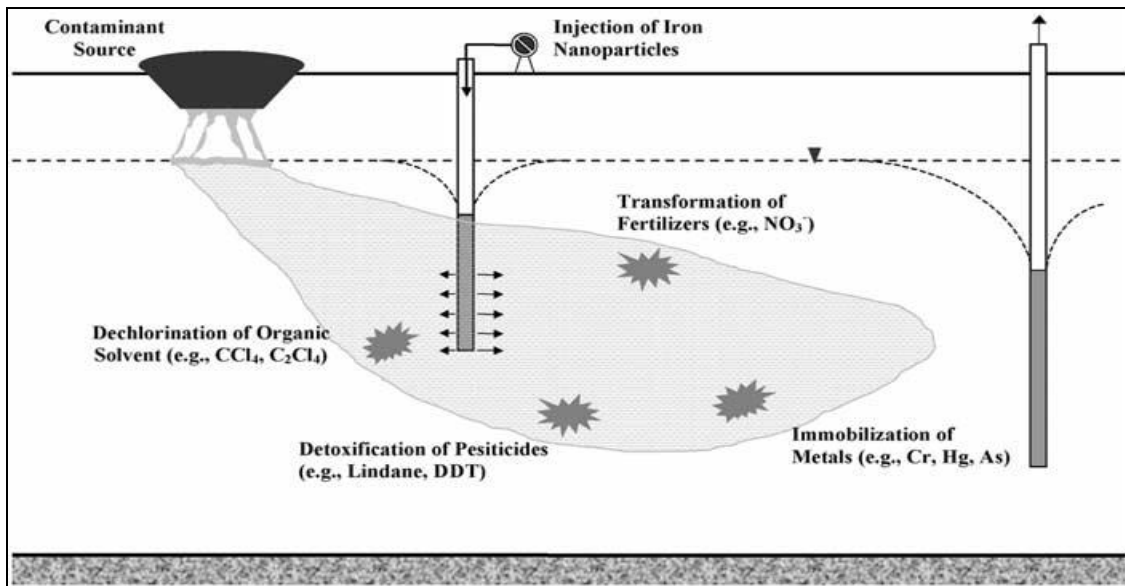


**Figure 3 Application of nZVI for in situ remediation. Source: Zhang (2003)**

Many researchers have demonstrated that nZVI and bimetallic nZVI is an effective tool for the remediation of groundwater and soil. nZVI may react with a broad range of environmental contaminants such as: chlorinated compounds (Wang & Zhang, 1997; Choe et al, 2000; Zhang, 2003; Lowry & Johnson, 2004; Liu et al., 2005), heavy metals (Ponder et al., 2000), and inorganics (e.g., arsenic) (kanel et al., 2005). Also nZVI has been applied for denitrification of lakes (Choe et al., 2000). nZVI and bimetallic nZVI reaction mechanism is surface-mediated, similar to ZVI. Table 7 shows a list of several contaminants to be treated by nZVI.

**Table 7 Environmental Contaminants reduced by nanoscale zero iron valent.**

<b>Chemical Group</b>	<b>Contaminant</b>	<b>Reference</b>
<b>Chlorinated methanes</b>		
	Carbon tetrachloride (CCl <sub>4</sub> )	(Elliott & Zhang, 2001) (Nurmi, et al., 2005)
	Chloroform (CHCl <sub>3</sub> )	(Elliott & Zhang, 2001)
<b>Chlorinated ethenes</b>		
	Tetrachloroethene (C <sub>2</sub> Cl <sub>4</sub> )	(Elliott & Zhang, 2001)
	Trichloroethene (C <sub>2</sub> HCl <sub>3</sub> )	(Li et al., 2003) (Liu et al, 2005)
	cis-Dichloroethene (C <sub>2</sub> H <sub>2</sub> Cl <sub>2</sub> )	(Elliott & Zhang, 2001)
	1,1-Dichloroethene (C <sub>2</sub> H <sub>2</sub> Cl <sub>2</sub> )	(Elliott & Zhang, 2001)
	Vinyl chloride (C <sub>2</sub> H <sub>3</sub> Cl)	(Elliott & Zhang, 2001)
<b>Polyhalogenated methanes</b>		
	Organochloride Pesticides	(Zhang W. , 2003)
	Polychlorinated biphenyl	(Wang & Zhang, 1997) (Lowry & Johnson, 2004)
<b>Heavy metal ions</b>		
	Arsenic (As(III), As(V))	(kanel et al., 2005)
	Lead (Pb(II))	(Ponder et al., 2000)
	Chromium (Cr(VI))	(Ponder et al., 2000)
<b>Inorganic anions</b>		
	Nitrate (NO <sup>-3</sup> )	(Choe et al., 2000)

Furthermore, the nZVI have been applied in microbiological treatment. Lee et al., (2008) have found that nZVI can inactivate *Escherichia coli* in aqueous solution. This aspect was observed under deaerated conditions. On the other hand, the inactivation under air-saturated conditions required much higher nZVI dose due to the corrosion and surface oxidation of nZVI by dissolved oxygen.

Naja et al., (2008) studied the degradation of hexahydro-1,3,5-trinitro-1,3,5-triazine (RDX), an explosive used in industrial and military facilities, with nanoscale zero valent iron in the presence and absence of stabilizer additive such as carboxymethyl cellulose (CMC) or poly(acrylic acid) (PAA). nZVI (3 g/L) completely degraded 82 μmol of RDX in five minutes under aerobic (98.3%) and anaerobic (100%) conditions.

One of the issues this technology has to overcome is the reduction of iron reactivity over time, probably due to the formation of surface passivation layers or due to the precipitation of metal hydroxides and metal carbonates on the surface of iron. This may be avoided by using bimetallic nZVI.

Many researchers (Wang & Zhang, 1997; Lien & Zhang, 1999; Xu & Zhang, 2000; Schrick, et al. 2002; He & Zhao, 2005; Tratnyek & Johnson, 2006) have reported that the addition of secondary metal such as: Pd, Ni and Ag, can dramatically increase the iron reactivity and less oxidation of iron core-shell occurs. When a secondary metal is deposited on the iron nanoparticle surface, a galvanic cell is formed and iron serves as electron donor.

Bimetallic nZVI has been used for dechlorination of chlorinated methanes (Lien & Zhang, 1999), chlorinated ethenes (Wang & Zhang, 1997) (Lien & Zhang, 2001) (Schrick et al., 2002), Tee et al. (2005), chlorinated ethanes (Lien & Zhang, 2005) and chlorinated benzenes (Xu & Zhang, 2000). In most of cases, the surface-area-normalized reaction rate constant ( $K_{sa}$ ) was 1-2 orders of magnitude higher compared to nZVI, showing a faster reactivity with contaminants. Also, the removal efficiency was higher than 80%.

## **2.4 ZVI-BASED OXIDATION PROCESS (ZVI/O<sub>2</sub>)**

### **2.4.1 Introduction**

Recently, a new ZVI-based oxidative process has been demonstrated in several pioneering investigations (Noradoun et al., 2003; Joo et al., 2004 and 2005; Feitz et al., 2005; Noradoun and Chen, 2005; Englehardt et al., 2007). At mild conditions (room temperature and atmospheric pressure), granular or nano-particulate ZVI activates O<sub>2</sub> to produce reactive oxidant species (ROS). ROS chemically destroys aqueous organic compounds through oxidation mechanisms (**Error! Reference source not found.**), rather than reduction, as utilized for the existing ZVI dechlorination process, or adsorption/coagulation due to iron corrosion products.

Compared with other remediation processes, the ZVI/O<sub>2</sub> process has attracted much attention due to three characterizations (Wang and Zang, 1997; Noradoun et al., 2003; Joo et al., 2004 and 2005; Feitz et al., 2005; Noradoun and Chen, 2005; Li et al., 2006; Englehardt et al., 2007). First, this process is able to effectively decompose a range of organic pollutants not amenable to reductive degradation (e.g. 1,2-dichlorethane) through chemical oxidation utilizing ROS. Second, this process is potentially cost-effective.

ROS is generated under mild reaction conditions, and even neutral pH. O<sub>2</sub> is obtained from easily accessible air. And no additional irradiation energy is required. Third, this process is environmentally friendly. Complex toxic organic compounds are degraded into simple and benign molecules, and even finally mineralized into inorganic water and some degradation byproducts, (Joo & Zhao, 2008; Joo et al., 2004). Iron sludge as ZVI corrosion product itself has no known toxic effect, considering that iron is one of the abundant elements on Earth.

#### **2.4.2 ROS Formation in ZVI/O<sub>2</sub> System.**

Two different reaction mechanisms occur in ZVI/O<sub>2</sub> system for oxidant production and reaction kinetics. Both are explained in Figure 4 **Error! Reference source not found.**. In the first mechanism, ZVI reacts with oxygen to produce hydrogen peroxide (H<sub>2</sub>O<sub>2</sub>) through transfer of two electrons (Reaction 1-3). In the second mechanism, ferrous iron (Fe<sup>2+</sup>) produced by ZVI oxidation reacts with oxygen during a several one-electron transfers to produce hydrogen peroxide (H<sub>2</sub>O<sub>2</sub>) (Reaction 4-5). The first mechanism is dominant under acidic conditions due to the reaction with O<sub>2</sub> is too slow.

On the other hand, the second mechanism is occurring under neutral to alkaline conditions and mostly in presence of iron corrosion products. Thereafter, H<sub>2</sub>O<sub>2</sub> oxidizes Fe<sup>0</sup>(s) without producing ROS (reaction 6) and the remaining H<sub>2</sub>O<sub>2</sub> reacts with Fe<sup>2+</sup> to yield ROS (Reaction 7) or an oxidizing agent that can also reacts with the contaminant. Simultaneously, some Fe(III) is precipitated in the form of iron sludge that may continue to influence the redox procedure through passivation and acting as a surface catalyst for Fe(II) oxidation by O<sub>2</sub>/H<sub>2</sub>O<sub>2</sub> (reaction 8).

ROS species in the ZVI/O<sub>2</sub> system likely depends on solution pH (Joo, 2004; Englehardt et al., 2007; Keenan, C., and Sedlak, D. 2008). Although the detailed procedure is little known, the dominant ROS produced are speculated to be hydroxyl radicals (OH•) at an acidic condition, and non-hydroxyl radical species (e.g. ferryl) at a neutral-weakly alkaline condition. At an acidic condition, OH• formed through the reaction 1, is detected through OH• scavenger tests or measuring the oxidation products of a variety of probe compounds (Joo, 2004; Joo, 2004; Feitz, et al., 2005).

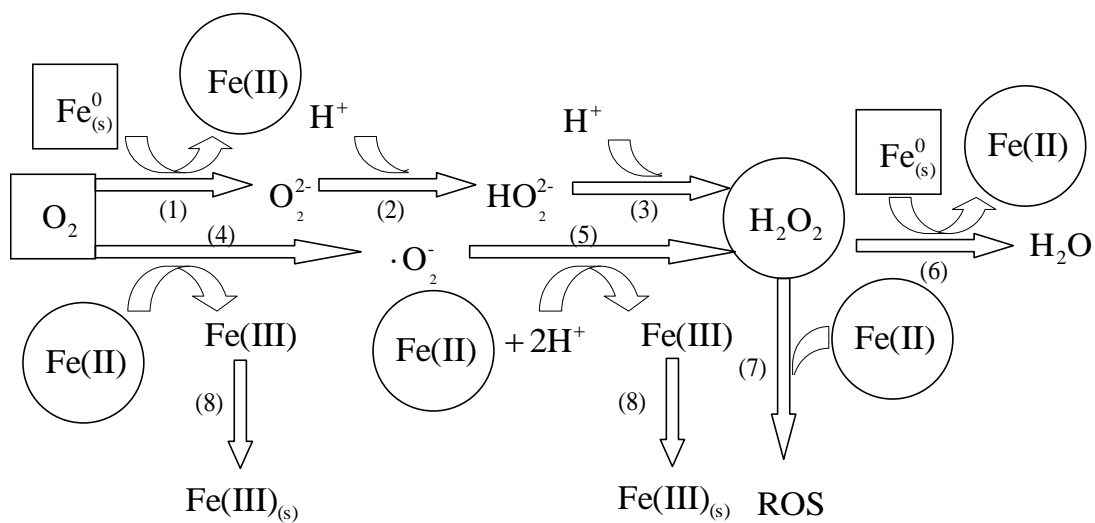
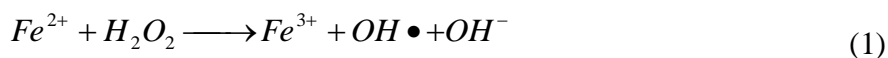


**Figure 4 Proposed primary reaction pathways in ZVI-mediated oxidation (Circle symbols indicate key intermediates; and square symbols indicate the reactants (Keenan & Sedlak, 2008). Fe(II) and Fe(III) represent total free, hydrolyzed and complexed ferrous and ferric species, respectively).**

### 2.4.3 Degradation of Contaminants via Oxidation

Zero valent iron in presence of oxygen has a great potential for degradation of organic compounds in groundwater and soil, including herbicides and chlorinated compounds. As explained before, it is plausible that the degradation is due to the reaction of an oxidant produced such as hydroxyl radical ( $\text{OH}\cdot$ ) with contaminants.

Noradoun et al. (2003) studied the destruction of chlorinated phenols with iron particles in the presence of ethylenediaminetetraacetic acid (EDTA) under aerobic conditions. Experiments were carried out at room temperature. An aliquot of iron particles (40-70 Mesh) were added to reactors containing 1.1 mM 4-chlorophenol or 0.61 mM pentachlorophenol and 0.32 mM EDTA at pH 5.5. 4-chlorophenol and pentachlorophenol were degraded completely after 4 hr and 70 hr, respectively. The degradation of 4-chlorophenol shows a pseudo-first-order reaction rate. Fe-EDTA complex might be decomposed with release of carbon dioxide, iminodiacetic, and oxalic acids from EDTA.

Zero valent iron has been used for degradation of the carbthiolate herbicide, molinate (Joo et al., 2004). Molinate and its byproducts were analyzed by solid-phase microextraction (SPME) and GC/MS. The molinate removal efficiencies (initial concentration = 100 ppb) were 70% and approximately 100%, when sample was sparged with air and pure oxygen within 3 hr, respectively. Although the degradation of molinate was observed at pH 4 and 8, the higher removal efficiency was achieved at acidic conditions. Also, molinate removal was improved with the increasing nZVI. Two intermediate species, ferrous ion and hydrogen peroxide, were regarded as the indispensable chemicals to produce ROS. Both of them were monitored at pH 4, ZVI concentration of 0.89, 1.79 and 2.68 mM and placed in an orbital shaker at 75 rpm with continuous mixing. Ferrous concentration ranged from 0.07 to 0.14 mM, and the hydrogen peroxide level was 5-6  $\mu\text{M}$ .

Similar results have been reported by Feitz et al., (2005). Under the conditions described previously (Joo et al., 2004), EDTA was added to enhance the formation of ROS. In a column test, rapid degradation of molinate was observed. The optimal column configuration (sand and gravel) exhibited a 90% removal in 3 hrs. These results elucidate the great potential of nZVI in presence of oxygen for degradation of contaminants.

The application of nZVI for oxidation of organic compounds was evaluated by Joo et al. (2005). The oxidation capacity of nZVI in presence of oxygen was analyzed through measurement of *p*-hydroxybenzoic acid (*p*-HBA), the transformation product of benzoic acid (BA), a probe compound. All the reactions were completed by adding nZVI to buffered solutions containing BA (10 mM) at different pH values (3, 5, and 8). The *p*-HBA was detected within the first 25 min, and was slowly increased after one day. The higher concentration of *p*-HBA was observed at pH 3. *p*-HBA yield was 25% higher than produced at alkaline conditions. In addition, several competitors were evaluated for the selectivity of oxidant. Aniline, *o*-hydroxybenzoic acid, phenol, and humic acid were added at pH 3 with 10 mM BA. The production of *p*-HBA decreased as competitors concentration increased.

## **2.5 METHODS FOR nZVI NANOPARTICLES SYNTHESIS**

Several methods for nanoparticles synthesis have been developed (Li et al., 2006). All of these methods are divided into two groups: physical and chemical synthesis methods. Table 8 lists the different methods applied for nanoparticles synthesis. The particle size reported in this table ranges from 0 to 300 nm. In most of cases, the particle size is uniformly distributed.

**Table 8 Methods for nanoparticles synthesis**

Method Group	Method	Particle Size (nm)	Size distribution	Reference
Physical	Inert Gas Condensation	17	Uniform	Sanchez-Lopez (1997)
		8 to 28	Uniform	Nakayama (1998)
	Severe Plastic Deformation			(Sus-Ryszkowska et al., 2004)
	High-Energy Ball Milling	10	Uniform	Del Bianco et al (1998)
		15 to 24		Malow et al. (1998)
	Ultrasound Shot Peening	10	Uniform	Tao et al. (1999)
Chemical	Reverse micelle (or microemulsion)	7 nm coated with 1 nm gold shell	Narrow	Carpenter (2001)
		< 10	-	Li et al (2003)
		3 nm Au core coated with 1 nm Fe	-	Wiggins (2000)
		10	Uniform	Song et al (2004)
	Controlled chemical coprecipitation	< 5	-	Liu et al (2004)
	Chemical vapor condensation	5 to 13	-	Choi et al (2001)
	Pulse electrodeposition	19	Uniform	Natter et al (2000)
	Liquid flame spray	40	-	Makela et al (2004)
	Liquid-phase reduction	60.2	-	Zhang (2000)
		1 to 100	-	Choe et al (2003)
		10 to 100	-	Kanel et al (2005)
	Gas-phase reduction	50 to 300	-	Nurmi et al (2005)

The liquid-phase reduction method is one of most commonly used in environmental applications due to its simplicity and productivity. Also known as borohydride reduction, the liquid phase reduction method was applied by Glavee et al. (1995). Generally, the particle synthesis is achieved by adding an aqueous solution of  $\text{NaBH}_4$  to  $\text{FeCl}\cdot 6\text{H}_2\text{O}$  or  $\text{FeSO}_4\cdot 7\text{H}_2\text{O}$  aqueous solution with continuous mixing. The reductant is stoichiometrically excessive relative

to all the ferric or ferrous ions. Moreover some health and safety conditions have to be taken into consideration in this process. The hydrogen gas is the main byproduct in liquid-phase reduction method; therefore it's mandatory to be completed in a fume hood and explosion-resistant mixers to avoid any kind of sparks production. This method would be used for the purpose of this research.

## 2.6 CHARACTERIZATION OF nZVI NANOPARTICLES

### 2.6.1 nZVI Core-shell Structure

The nZVI is characterized by a core-shell structure composed of ZVI in the center and iron oxidation products covered on the ZVI surface. The typical core-shell structure is shown in Figure 5. ZVI, used by different researchers, has different particle sizes, size distribution, surface area and shape. These key physical and chemical characteristics are related to the nanoparticles reactivity

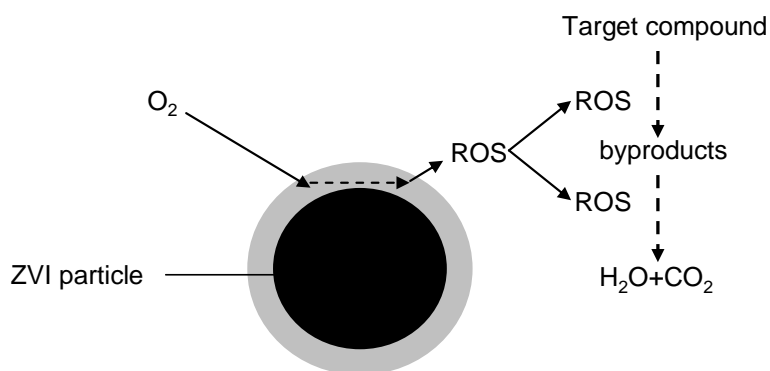


**Figure 5 nZVI core-shell structure and the conceptual reaction diagram of nZVI/O<sub>2</sub> system. Particle size and shell thickness ranges around 20-40 nm and 2-3 nm (Li, 2005; Liu, 2005; Nurmi, 2005), respectively**

Nurmi et al. (2005) analyzed nanoparticles structure using the borohydride reduction. Structure information regarding particle size and crystallinity was obtained with transmission

electron microscopy (TEM) and X-ray diffraction (XRD), respectively. TEM analysis revealed three levels of structure: 1) small crystallites < 1.5 nm, 2) 20-100 nm spherical aggregates with an amorphous coating and 3) chains of 20-100 nm particles. The cores either are made of very small grains or are amorphous, and the shells are apparently amorphous. XRD patterns shows that the mean crystalline size was <1.5 nm, and the initial zero valent iron content ranged within  $97 \pm 8\%$  (Liu et al., 2005).

### **2.6.2 Specific Surface Area**

One of the most important factors affecting the chemical and physical properties of nanoparticles is the specific surface area. Surface area of nZVI is determined with the BET method (Brunauer–Emmett–Teller isotherm Method). The BET isotherm is the basis for determining the level of nitrogen adsorption on a given surface.

It has been demonstrated that nanoparticles with larger specific surface area, have greater rates of reaction with contaminants (Nurmi et al., 2005). Larger specific surface area makes nanoparticles stronger reductants for a great variety of contaminants.

Zhang et al. (1998) found that nanoscale metal particles exhibited higher surface areas (1-2 orders higher) than microscale ones. Higher specific areas provided more reactive sites for reaction, and offer higher reaction rates (Zhang, 2003 and Nurmi et al., 2005). Nurmi et al. (2005) explained that the enhanced reactivity of nZVI might be attributable to higher density of reactive surface sites and also greater intrinsic reactivity of surface sites. Table 9 shows shape and surface area of bimetallic or metal-coated nanoparticles, reported by several researchers.

**Table 9 BET surface area and shapes for different samples. Source: Liu, 2005.**

<b>Sample</b>	<b>Specific surface area (m<sup>2</sup>/g)</b>	<b>Shape</b>	<b>Remark</b>	<b>Reference</b>
Fe	N/A	Not spherical	As prepared	Signoretti (2003)
<i>a</i> Fe <sup>H2</sup>	29	Irregular	As received	Nurmi (2005)
<i>b</i> Fe <sup>BH</sup>	33.5	Irregular	As received	Nurmi (2005)
Fe	33.5	Not spherical	Borohydride reduction	Wang (1997)
Pd/Fe	35 ± 2.7	Roughly spherical	Borohydride reduction	Zhang, 2003 and Lien 1999
Fe	31.4	N/A	Borohydride reduction	Choe (2000)
Fe	24.4 (unreacted) 37.2 (corroded)	Amorphous	Borohydride reduction	Kanel (2005)
Fe	24.4 ± 1.5 (ferragel)	N/A	Borohydride reduction	Ponder (2000)
Fe	21.7 ± 1.5 (unsupported) 13.87 and 15.08 for 2 samples	Irregular	Hard sphere model and 7.87g/m <sup>3</sup> for Fe	Kecskes (2003)
Fe	24.4 ± 1.5 (supported) 21.7 ± 1.5 (unsupported)	Irregular	85% Fe <sub>0</sub>	Ponder (2001)
Fe	33.9	N/A	N/A	Zang (1998)
Fe/Ag	35	Irregular	Iron core + Silver shell	Xu (2000)
Fe	18	N/A	83% Fe'	Schrick (2002)
Ni/Fe	59	Not spherical	53.1% FeO, 15.6% Ni	Schrick (2002)

*a*, commercial available iron nanoparticles.

*b*, iron nanoparticles synthesized by liquid-phase reduction.

### 3. MATERIALS AND METHOD

#### 3.1 Chemicals

All the chemical reagents were of analytical grade, except noted. 2-propanol, 2,4-dinitrophenyl hydrazine (DNPH), acetone (HPLC grade), formaldehyde (37% aqueous sol.), MES monohydrate, perchloric acid(60-65%), sodium acetate trihydrate, sodium tetraborate decahydrate and sodium borohydride (98%) were obtained from Alpha Aesar. Acetonitrile (HPLC grade), N, N-diethyl-p-phenylenediamine (DPD), poly (acrylic acid) (50% solution), sodium phosphate dibasic, sodium tetrachloropalladate were purchased from Acros Organic. Hydrogen peroxide (30%), hydrochloric acid (6N), methanol (HPLC grade) and sodium hydroxide (0.5 N) were purchased from Fisher. Nickelous sulfate hexahydrate and piperazine-N, N'-bis(2-ethanesulfonic acid) (PIPES) were obtained from JT Baker. All solutions were prepared with ultrapure water (Millipore, 18.2M $\Omega$ ).

#### 3.2 Synthesis of nZVI and bimetallic nZVI

nZVI was synthesized using a modified method originally developed by Wang and Zhang (1997). 0.1 M ferric chloride hexahydrate ( $\text{FeCl}_3 \cdot 6\text{H}_2\text{O}$ ) was made by dissolving 0.2702 g  $\text{FeCl}_3 \cdot 6\text{H}_2\text{O}$  into 10 mL  $10^{-4}$  HCl  $\text{N}_2$ -sparging solution, and then stored in 40 mL glass vial. And 0.3 M sodium borohydride ( $\text{NaBH}_4$ ) was made by dissolving 0.11 g  $\text{NaBH}_4$  in 10 mL DI water. Excess  $\text{NaBH}_4$  was used to guarantee that all  $\text{Fe}^{3+}$  was reduced to  $\text{Fe}^0$ .

$\text{NaBH}_4$  solution was added dropwise to the  $\text{FeCl}_3$  solution at room temperature and atmospheric pressure in a vortex shaker. Shaking and dropwise addition ensured production of uniform and dispersed ZVI nanoparticles in the solution. Nanoscale ZVI particles were produced through reduction of  $\text{Fe}^{3+}$  by  $\text{NaBH}_4$ , as shown below.



After addition of sodium borohydride solution, black-gray solid particles immediately appeared (Figure 6). 5-10 min after the  $\text{NaBH}_4$  and  $\text{FeCl}_3$  were completely mixed, particles were separated from liquid phase by placing a strong magnet in the bottom of glass vial for 3 min, and the supernatant was decanted to remove chloride from the solution. Subsequently, the particles were washed at least 3 times with  $10^{-4}$  HCl  $\text{N}_2$ -sparging solution to prevent rapid oxidation of iron nanoparticles. Ultrasonic bath was used to break nanoparticles for 20 min. The final concentration of nZVI in this mixture was 50 mM (2.8 g/L).

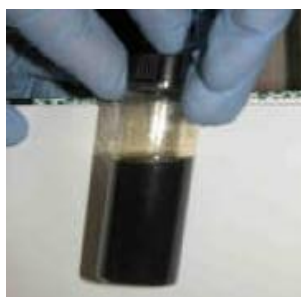


**Figure 6 nZVI particles suspension**

Bimetallic nanoparticles synthesis was achieved by the following modified nZVI synthesis method. Just after the  $\text{Fe}^{3+}$  was reduced by  $\text{NaBH}_4$  to synthesize nZVI as described above, a secondary metal ion solution was dropwise introduced into the suspended nZVI solution. The secondary metal was reduced by nZVI, so that the elemental secondary metal was coated on the nZVI surface. Three different secondary metals were used in this study: Pd, Ni and Ag. The studied molar ratio of secondary metal to nZVI were 1%, 5% and 10%, respectively.

Preparation of Pd, Ni, and Ag stock solutions was achieved by dissolving 2.63 g, 0.2942 g and 1.6987 g of nickel sulfate ( $\text{NiSO}_4 \cdot 6\text{H}_2\text{O}$ ), sodium tetrachloropalladate ( $\text{Na}_2\text{PdCl}_4$ ) and silver nitrate ( $\text{AgNO}_3$ ), respectively, into 50 mL DI water. The desirable secondary metal to Fe molar ratios was obtained by diluting these stock solutions into 5 ml DI water. **Table 10** shows the dilution factors for each metal.

**Table 10 secondary metal content and dilution factor for bimetallic nZVI.**

	[Pd]/[Fe]				[Ni]/[Fe]				[Ag]/[Fe]		
	1%	5%	10%		1%	5%	10%		1%	5%	10%
<b>Na<sub>2</sub>PdCl<sub>4</sub> Solution (mL)</b>	0.5	2.5	5	<b>NiSO<sub>4</sub>·6H<sub>2</sub>O Solution (mL)</b>	0.05	0.25	0.5	<b>AgNO<sub>3</sub> Solution (mL)</b>	0.05	0.25	0.5
<b>DI Water (mL)</b>	4.5	2.5	0	-	4.95	4.75	4.5	-	4.95	4.75	4.5
<b>Dilution Factor</b>	1/10	1/5	1/1 (no dilution)	-	1/100	1/20	1/10	-	1/100	1/20	1/10

5 mL secondary metal solution was added dropwise to 20 mL Fe nanoparticles solution on a vortex shaker. Then, the solution was shaken for a while and stood for 5 min to ensure that all secondary metal ions were reduced and deposited on the surface of Fe nanoparticles as follows.



Because the addition of the secondary metal solution to the nZVI suspension increased the total volume to 25 mL, the final concentration of bimetallic nZVI was 40 mM.

### 3.3 Morphology of nZVI particles

In this study, scanning electron microscope (SEM) analysis was used to characterize the morphology of the synthesized nanoparticles. To prevent aggregation of these nanoparticles, the nZVI synthesis procedure was slightly modified based on the method used by Huang and Ehrman (2007). 0.135 g of ferric chloride hydrate was dissolved in 10 mL of deionized water and 10 mL of poly (acrylic) acid (PAA) solution (3.5% wt. diluted from 50% wt solution) was added. PAA acted as a dispersing agent to prevent possible particle aggregation. Thereafter, 0.375 g of

sodium borohydride was dissolved in 5 mL of DI water. Then sodium borohydride solution was added to the ferric chloride-PAA solution dropwise. The following steps are the same as those to synthesize bare nZVI particles, as mentioned previously. The nZVI synthesis reaction produced numerous bubbles. The reaction was completed when bubbling stopped. Finally, particles were dried with nitrogen to prevent any oxidation.

The mean size, distribution and morphology of nanoparticles, their most important physical properties, were analyzed with a SEM (JEOL-JSM-6930LV). A SEM was operated with a beam of electrons, called primary electrons, to raster the surface of a sample and to excite surface electrons, called secondary electrons. The secondary electrons are registered by a detector, which then generates a topographic image of the surface. The images produced have good depth of field, which allows visualization of the surface in a near 3-D quality. This is due to the differences in surface height at which the secondary electrons are emitted (Figure 7 ).

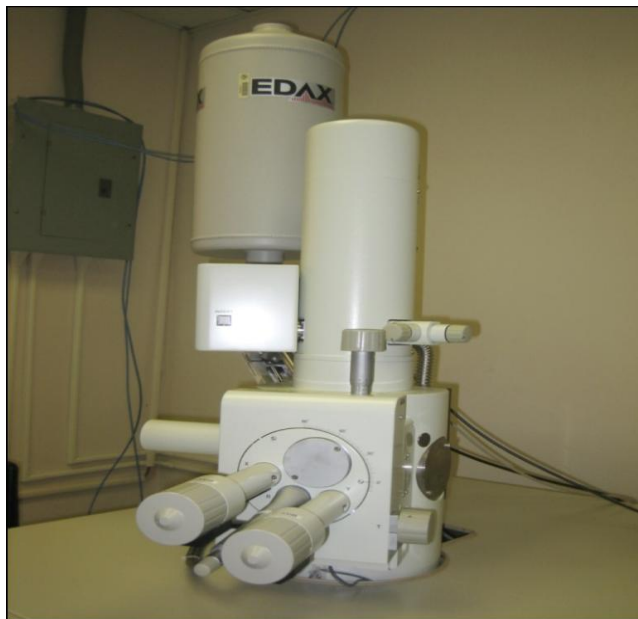


**Figure 7 Scanning Electron Microscope (SEM)**

### 3.4 Batch Experiments

All the experiments were carried out at room temperature in 73.5 mL glass serum vials containing a probe compound. Two probe organic compounds were used to quantify the reactive oxidant species, methanol and 2-propanol. These vials were sealed and had no headspace to avoid transfer of O<sub>2</sub>, VOCs (probable oxidation byproducts of the probe compound), and any other gas from or into the vials. Every vial was installed in a water bath shaker at 150 rpm and 25<sup>0</sup>C to keep particles in suspension and a complete-mixing (Figure 8). All reactions were completed by addition of 400 μM nZVI or bimetallic nZVI to O<sub>2</sub>-saturated pH buffered solutions (pH 3-9) containing probe compounds (195 mM methanol and 250 mM 2-propanol) (Figure 9).



**Figure 8 Serum vials filled with O<sub>2</sub>-saturated pH buffered solutions**



**Figure 9 Vials in a water bath shaker**

Solution pH was maintained with the following buffer solutions: sodium acetate (pH 4-5.5), 2-(N-morpholino) ethanesulfonic acid (pH 6)(MES), piperazine-N, N'-bis (ethanesulfonic acid) (pH 6.5-7.5)(PIPES), and sodium borate (pH 8-9). MES and PIPES were used because they form no complexes with metals including iron (Yu et al., 1997). Solutions at pH 3 were

unbuffered. All buffer concentrations were 8 mM. When needed, pH was adjusted using 1 N H<sub>2</sub>SO<sub>4</sub> (Acros Organics) or 0.5 N NaOH (Fisher). The reaction time proceeded for 3 hours. At least two reactors were sacrificed for measurement of concentrations of oxidation byproducts, and 5 mL sample was collected from each reactor with a 5 mL syringe and filtered through a 0.22 μm nylon syringe filter.

### **3.5 Quantification of Reactive Oxidant Species (ROS)**

The measurement of ROS was achieved by a modified method initially developed by Keenan and Sedlak (2008). The yields of oxidation products of different probe compounds were measured at an acidic to weakly basic pH range. As explained above, two probe organic compounds were used, methanol and 2-propanol. Methanol can be degraded to formaldehyde (HCHO) by OH· or ferryl ions (Asmus and Möckel, 1973; Hess and Tully, 1989), while 2-propanol is selective for OH· with an oxidation byproduct of acetone (CH<sub>3</sub>COCH<sub>3</sub>) (Asmus and Möckel, 1973). Quantification of these oxidation byproducts provided an insight into the yields and species of ROS generated at different experimental conditions. Formaldehyde and acetone were measured by using 2,4-dinitrophenylhydrazine (DNPH) derivatization of HCHO with analysis by HPLC equipped with UV detector (Grannas and Martin, 2006). The ROS yields were quantified by measuring the concentrations of these oxidation byproducts.

#### **3.5.1 2,4-dinitrophenylhydrazine (DNPH) Derivatization of Aldehydes and Ketones**

2,4-Dinitrophenylhydrazine can be used to qualitatively detect the carbonyl functionality of a ketone or aldehyde functional group. The mechanism for the reaction between 2,4-dinitrophenylhydrazine and an aldehyde or ketone is shown below:

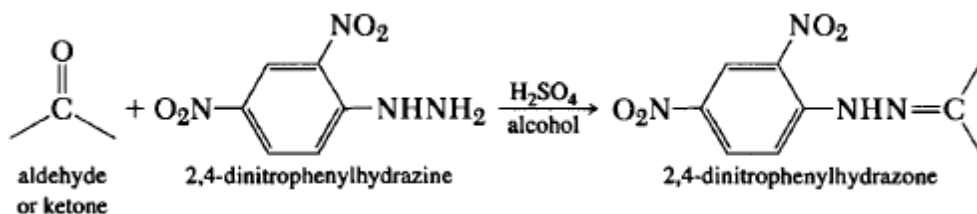


**Figure 10 Reaction Mechanism between 2,4 DNPH and aldehyde or ketone. Source: Shriner et al., (2004)**

Shriner et al., (2004) explained that the color of a 2,4-dinitrophenylhydrazone elucidates the structure and source of the aldehyde or ketone. The dinitrophenylhydrazones of non-conjugated aldehydes and ketones with another functional group are yellow. Generally, a yellow dinitrophenylhydrazone may be assumed to be unconjugated. However, an orange or red color should be interpreted with caution, since it may be due to contamination by an impurity.

In this study, the 2,4 DNPH derivatization was completed by adding a DNPH solution to the samples (Grannas and Martin, 2006). The DNPH solution was prepared through adding excess DNPH to acetonitrile to make saturated DNPH solution. The upper saturated solution was diluted in acetonitrile (dilution factor of 1/20).

### 3.5.2 Separation of Aldehyde and Ketone Hydrazone by High performance Liquid chromatography (HPLC) and UV detection

Formaldehyde and acetone hydrazones were separated from excess DNPH through high performance liquid chromatography followed by UV absorbance detection (Pelkin Elmer Series 200). Every 2-mL Vial for HPLC analysis of samples was set with the following solutions:

- DNPH solution: 0.20 mL
- 1N H<sub>2</sub>SO<sub>4</sub>: 0.20 mL
- Ethanol: 0.20 mL
- Water sample: 1.4 mL

Separation was achieved using a C-18 column with a guard column. The HPLC test method was configured as follows:

- Absorbance detection: 360 nm.
- Mobile phase: water: 60%; acetonitrile: 40%.
- Run isocratically at a mobile phase flow rate of 1 mlmin<sup>-1</sup>.
- Retention time: 8 min.
- Injection volume: 25 µL.

For the calibration of HPLC, 0.1875 mL of Formaldehyde solution (37% vol.) was diluted by DI water to 25 mL 0.10 M HCHO. Meanwhile, 73.53 µL of acetone (>99%, HPLC grade) was diluted into 25 mL of deionized water to make 0.01 M C<sub>3</sub>H<sub>6</sub>O. Both solutions were diluted into 0, 25, 50, 100 µM of HCHO and C<sub>3</sub>H<sub>6</sub>O, respectively. Their calibration curves are shown in Figure 11 and Figure 12.

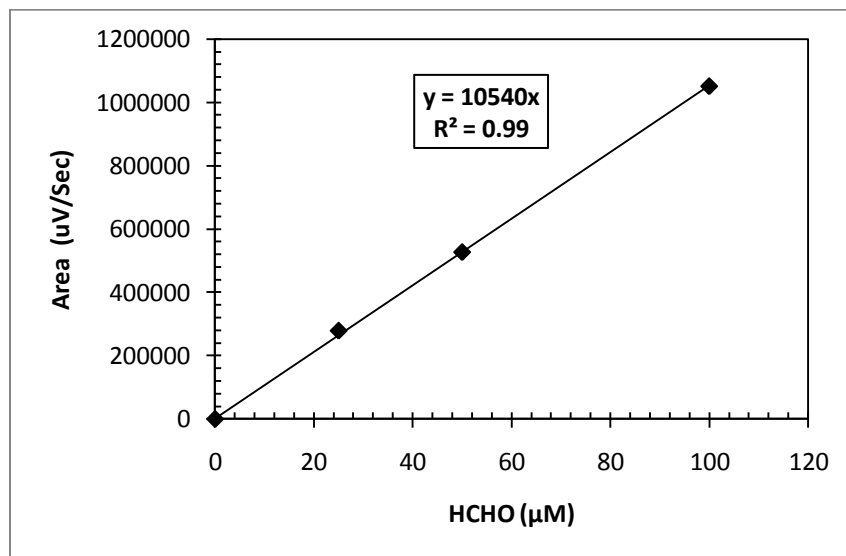


**Figure 11 HCHO calibration curve**

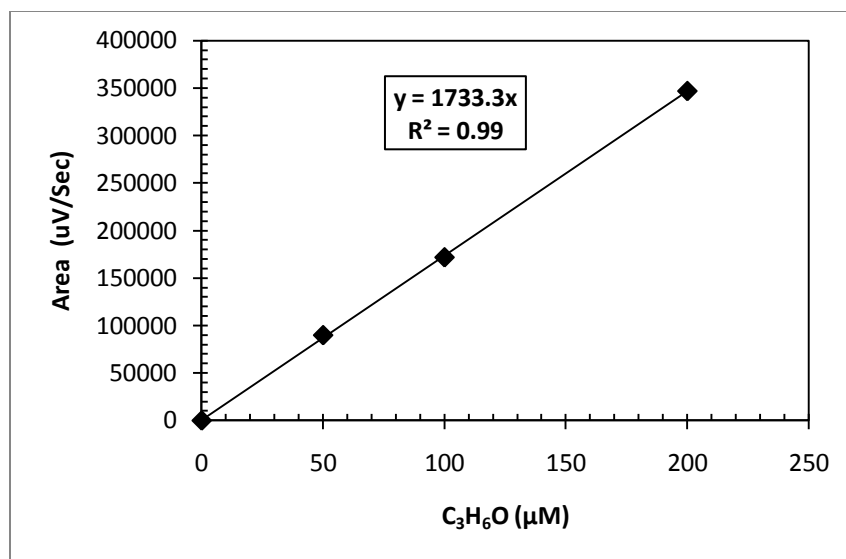


**Figure 12 C<sub>3</sub>H<sub>6</sub>O Calibration curve**

### **3.6 Measurement of Hydrogen Peroxide (H<sub>2</sub>O<sub>2</sub>) and Ferrous Iron (Fe<sup>2+</sup>)**

Hydrogen peroxide and ferrous iron are key intermediate compounds since they react with each other to produce ROS. Therefore, a study to further investigate levels of the both species produced in the bimetallic nZVI/O<sub>2</sub> system helped better understand the oxidative mechanism of the process. All the tests were conducted in the reactors described above. The experimental procedure is also identical with that described above, except that a probe compound-free solution was used and that dissolved Fe(II) and H<sub>2</sub>O<sub>2</sub> were measured after sampling.

For each metal additive type, a set of full-factorial experiments were conducted at seven reaction times with control (0.5, 1, 5, 10, 30, 60, 180 min). The pH and metal additive content were the optimal levels determined in previous experiment (Quantification of ROS). The initial nZVI concentration will be fixed at the level used previously. In the control experiments, the bimetallic nZVI particles was replaced with bare nZVI particles.

H<sub>2</sub>O<sub>2</sub> was measured spectrophotometrically using the DPD method (Brader et al., 1988) as modified by Voelker and Sulzberger (1996) to minimize interference by Fe(II) and Fe(III). Bipyridine was added to complex Fe(II), and EDTA was added to complex Fe(III). Because bipyridine forms a colored complex with Fe(II), this experimental method also can be applied for simultaneous Fe(II) measurement.

The procedure consisted of the following steps: 0.25 mL of bipyridine stock (0.01 M bipyridine in approximately 10<sup>-3</sup>M HClO<sub>4</sub>) and 1.00 mL of pH 6 phosphate buffer (0.5 M total phosphate) were premixed in a vial, to which 5 mL of the sample was then added, followed by 0.05 mL of EDTA stock (10<sup>-2</sup> M Na<sub>2</sub>EDTA). After 60 s, for the Fe(II) measurement, absorbance was measured at 522 nm. Then, 2 mL of the DPD reagent (3.8 x 10<sup>-2</sup> M in 0.1 M H<sub>2</sub>SO<sub>4</sub>) was added, followed by 1 mL of the horseradish peroxidase reagent (100 unit/mL), and the absorbance at 551 nm was measured after 45 s for hydrogen peroxide.

For calibration of spectrophotometer, 0.0278 g of ferrous sulfate heptahydrate was dissolved into 100 mL DI water to make 1mM FeSO<sub>4</sub>·7H<sub>2</sub>O stock solution, and 11.34 mL of hydrogen peroxide solution (30%) was diluted into 100 mL (1mM). Both solutions were properly diluted by DI water to produce ferrous ion and hydrogen peroxide calibration standard curves (0, 25, 50, 75, μM), respectively (Figure 13 and Figure 14).

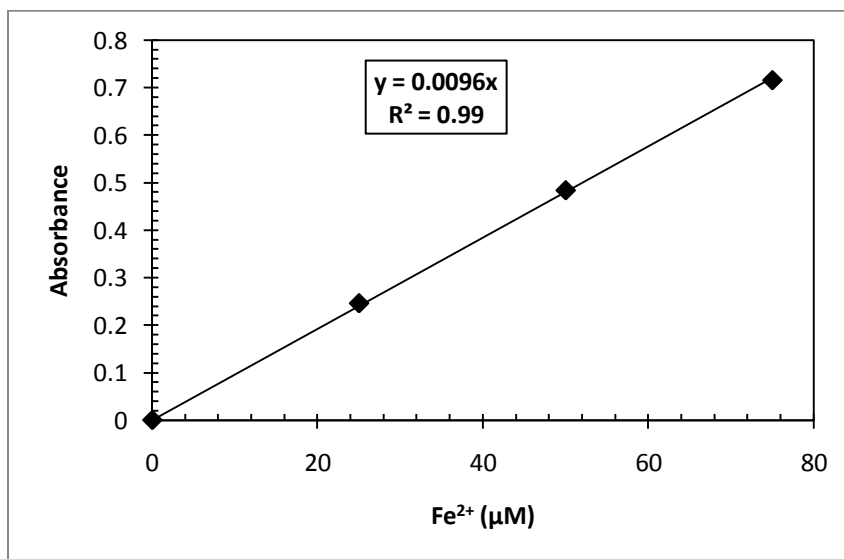


**Figure 13 Ferrous Calibration Curve**

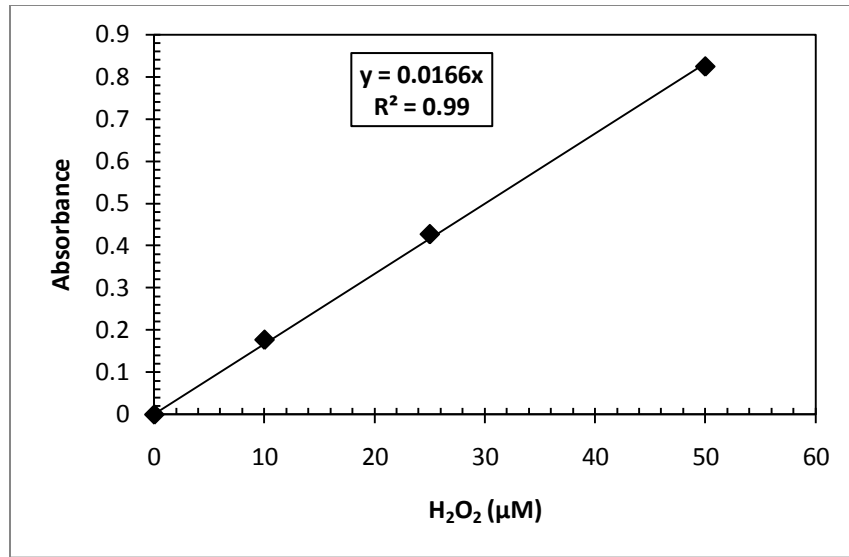


**Figure 14 Hydrogen Peroxide Calibration Curve**

## 4. RESULTS

### 4.1 Characterization of Nanoparticles

SEM images of freshly synthesized ZVI nanoparticles with 9000X and 10000X are shown in Figures 15 (a)-(b), respectively. As seen, these nanoparticles were well-dispersed. The SEM images with higher magnifications (20000X and 35000 X) are shown in Figure 16 (a)-(b). Roughly, the ZVI nanoparticles were spherical, with the diameters ranging within 20 - 200 nm. Some of them were aggregated to form clusters due to the magnetic properties of iron (Nurmi et al., 2005).

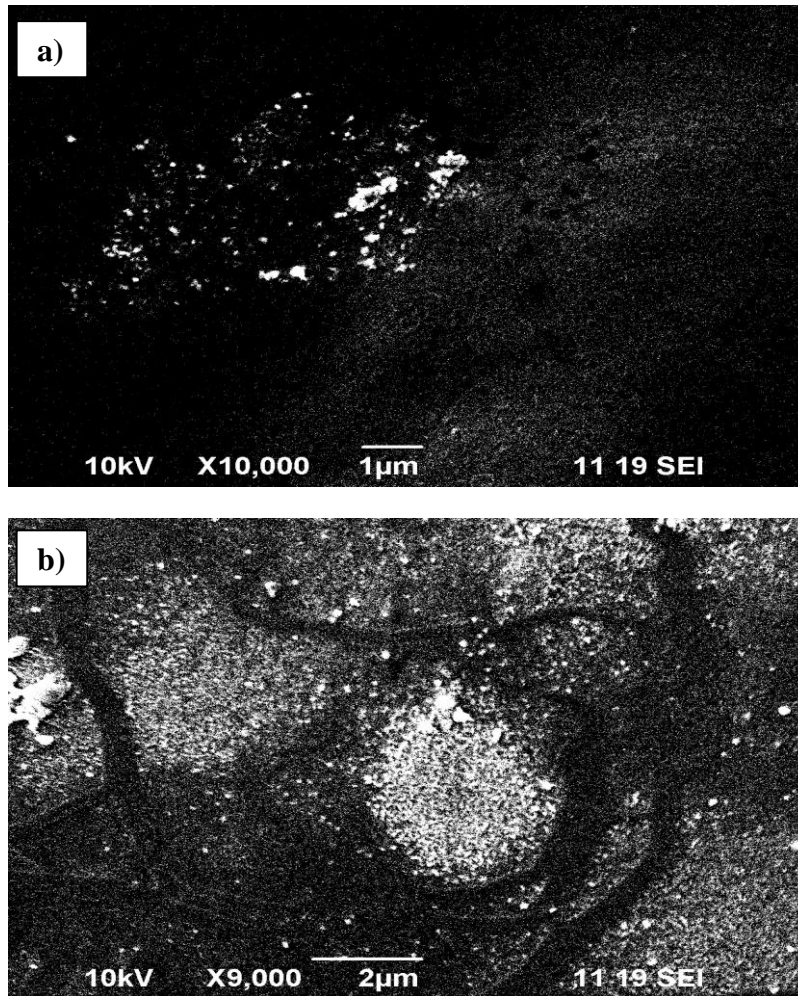


**Figure 15 SEM images of iron nanoparticles at a) 10000X and b) 9000X magnification**

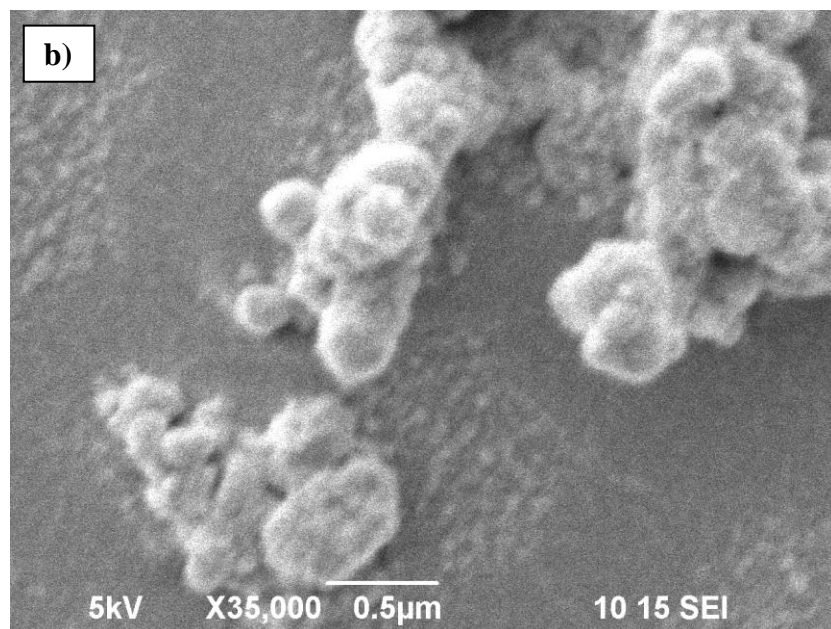
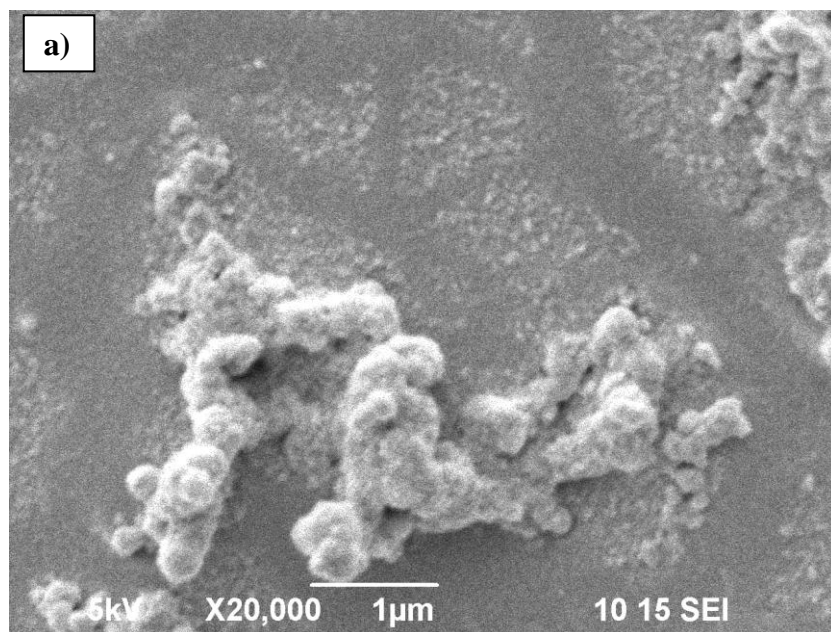


**Figure 16 SEM images of iron nanoparticles at a) 20000X and b) 35000X magnification**

## 4.2 Quantification of HCHO

The production of HCHO, from the oxidation of methanol at pH 6 was shown in Figure 17. HCHO was rapidly produced within 1 min in nickel, palladium and silver iron bimetallic nanoparticles activated by oxygen (Ni-Fe/O<sub>2</sub>, Pd-Fe/O<sub>2</sub>, and Ag-Fe/O<sub>2</sub>). As seen, the production of HCHO corresponds to 4.54, 20.21 and 24.62  $\mu\text{M}$  within 1 min, respectively. At 60 min, the yields of HCHO quickly increased in Ag-Fe/O<sub>2</sub> and Ni-Fe/O<sub>2</sub> to 44.28 and 16.72  $\mu\text{M}$ , respectively, corresponding to 3.68 and 1.79 times as that ( 23.81  $\mu\text{M}$ ) of Pd-Fe/O<sub>2</sub> .

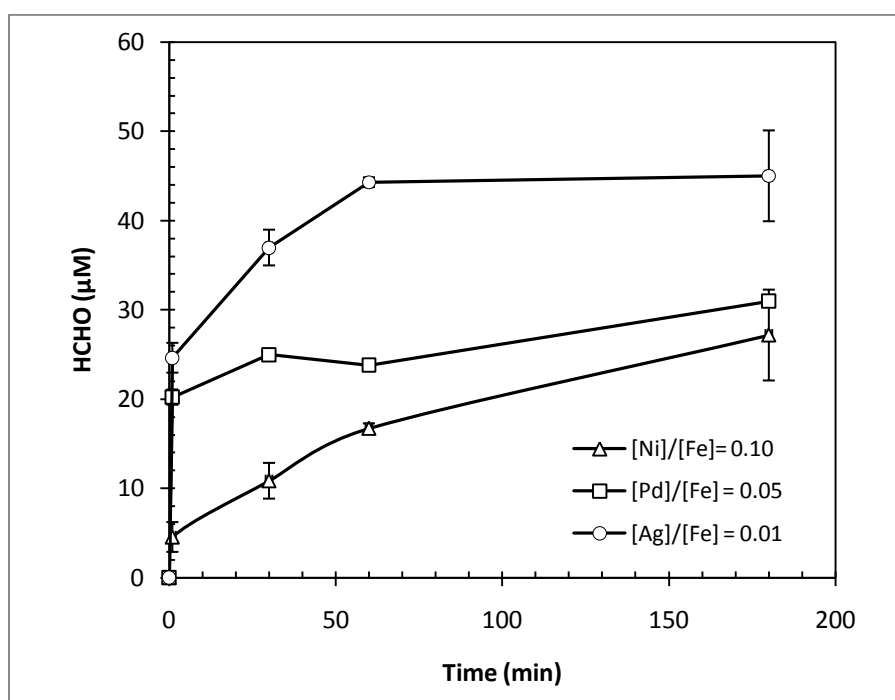


**Figure 17** Production of HCHO from [Ni]/[Fe]= 0.10, [Pd]/[Fe] = 0.05, [Ag]/[Fe] = 0.01 over time. CH<sub>3</sub>OH Initial Concentration = 195  $\mu\text{M}$ ; [Fe<sup>0</sup>] = 400  $\mu\text{M}$ ; pH = 6.

Over 180 min reaction time, HCHO continued to be produced in Ni-Fe/O<sub>2</sub> and Pd-Fe/O<sub>2</sub> systems that generated 10.45 and 7.15  $\mu\text{M}$  HCHO, respectively, more than those produced in 60 min (27.16 and 30.96  $\mu\text{M}$ ). In contrast, Ag-Fe/O<sub>2</sub> system did not significantly produce more HCHO (only 1  $\mu\text{M}$  increase). However, the highest yield of HCHO from oxidation of methanol

occurred in the Ag-Fe/O<sub>2</sub> system which produced 17.84 μM and 14.03 μM more HCHO than Ni-Fe/O<sub>2</sub> and Pd-Fe/O<sub>2</sub> system, respectively

#### **4.2.1 Effects of Secondary Metal Content and Solution pH in The Overall HCHO Production**

In this study, almost all the ROS could be trapped by methanol that was oxidized to (HCHO). Therefore, the level of HCHO produced reflected the ROS yield. For Pd-Fe nanoparticles, the HCHO production at different pH and secondary metals contents is shown in Figure 18. The pH levels were varied at 3, 4, 5, 6, 7, 8, and 9. And the molar secondary metal contents studied were 0 (for bare nZVI), 0.01, 0.05, and 0.10. As shown, the ROS production was pH-dependent. Over the entire pH range, the Pd-Fe nanoparticles appeared to produce more HCHO for any Pd content in most cases.

A typical trend of HCHO production at different pH is that the HCHO level increased with the increasing pH from pH 3, peaked at a circumneutral level (pH 5 or 6), and thereafter decreased when the pH continued increasing to 9. The highest HCHO levels for bare nZVI (BnZVI) and 0.05 Pd-Fe nanoparticles were 34 and 27 μM, respectively, occurring at pH 6. And the maximum HCHO level for 0.01 Pd-Fe nanoparticles was observed at pH 5 (31 μM). Interestingly, 0.10 Pd-Fe nanoparticles achieved the highest HCHO at pH 5 and 6, of which values were 31 μM. Compared with bare nZVI, Pd-Fe nanoparticles produced 15%, 25%, and 15% more HCHO at 0.01, 0.05, and 0.10 Pd content, implying that addition of Ni was able to yield more ROS.

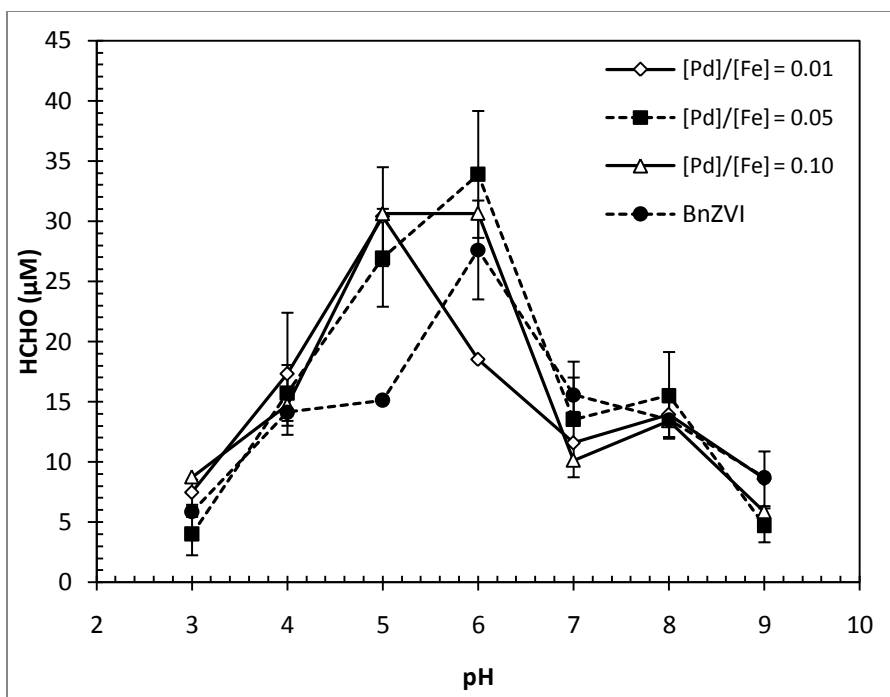


**Figure 18 Production of HCHO from [Pd]/[Fe]= 0.01, [Pd]/[Fe] = 0.05, [Pd]/[Fe] = 0.10. CH<sub>3</sub>OH Initial Concentration = 195 µM; [Fe<sup>0</sup>] = 400 µM; Reaction Time = 180 min**

For Ni-Fe nanoparticles, the HCHO production at different pH and secondary metals contents is shown in Figure 19. The levels of pH and secondary metals were identical with those used in the Pd –Fe tests. HCHO produced from Ni-Fe nanoparticles exhibited a similar pattern with that from Pd-Fe nanoparticles. The difference is that the maximum HCHO levels at the three different Ni contents all occurred at pH 6. The highest HCHO levels were 29, 34 and 53 µM for [Ni]/[Fe] = 0.01, 0.05, and 0.10, respectively, of which all were above 27 µM achieved from BnZVI. Therefore, the Ni coating on the nZVI surface improved the ROS yield.

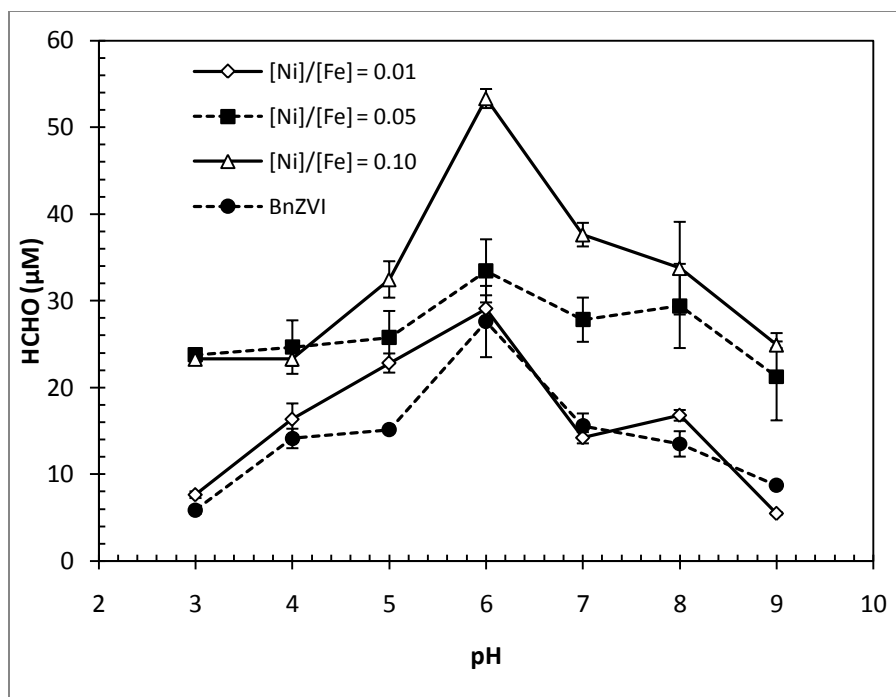


**Figure 19 Production of HCHO from [Ni]/[Fe]= 0.01, [Ni]/[Fe] = 0.05, [Pd]/[Ni] = 0.10. CH<sub>3</sub>OH Initial Concentration = 195 µM; [Fe<sup>0</sup>] = 400 µM; Reaction Time = 180 min**

For Ag-Fe nanoparticles, the HCHO production at different pH and secondary metal contents is shown in Figure 20. Similar to the other two secondary metal-coated iron nanoparticles, in most cases, the Ag-Fe nanoparticles produced more HCHO than BnZVI over the entire pH range. At any Ag content, the HCHO level was increased with the increasing pH from pH 3, peaked at pH 5 or 6, and then decreased when the pH was increased 7. Of note, the HCHO had a slight increase when the pH increased from 7 to 8, and then dropped when pH continued increasing to 9. This finding was not observed for the Pd-Fe and Ag-Fe nanopartilces. The highest HCHO level (52 µM) for [Ag]/[Fe] = 0.01 occurred at pH 6. In contrast, the HCHO levels of 31 and 49 µM for [Ag]/[Fe] = 0.05 and 0.10 peaked at pH 5, respectively. All of the HCHO production levels were greater than 27 µM achieved from BnZVI, suggesting the enhancement effect of Ag in the ROS production.

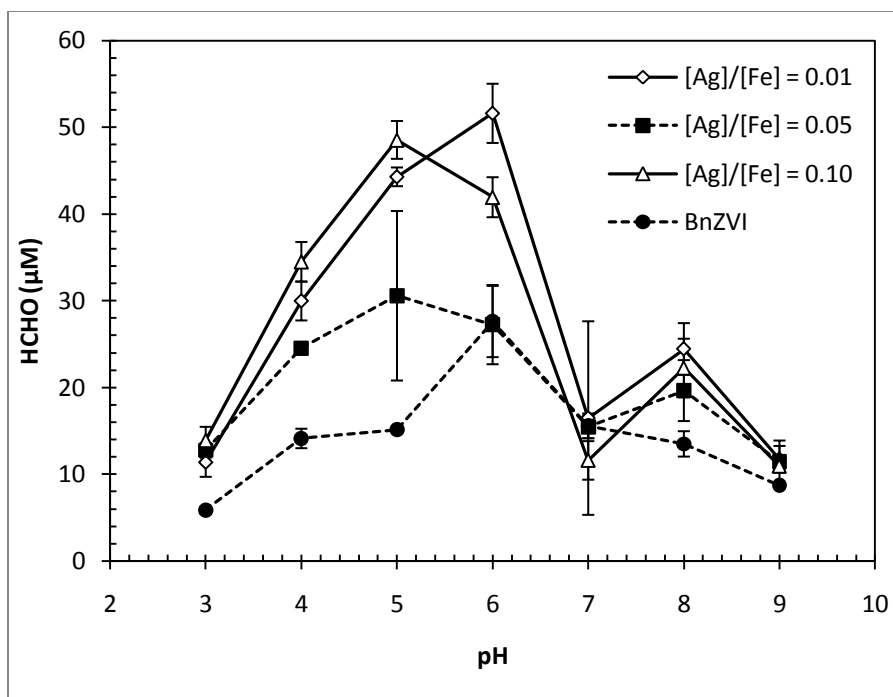


**Figure 20 Production of HCHO from [Ag]/[Fe] = 0.01, [Ag]/[Fe] = 0.05, [Ag]/[Ni] = 0.10. CH<sub>3</sub>OH Initial Concentration = 195 μM; [Fe<sup>0</sup>] = 400 μM; Reaction Time = 180 min**

To sum up, addition of Pd, Ni, and Ag to nZVI surface enhanced the production of ROS, to different degrees. Typically, the highest ROS yield occurred at weakly acidic conditions (pH 5-6), regardless of additive species and its content. The optimal pH range observed in this study may be attributable to the maximum oxidizing rate of Fe<sup>2+</sup> by O<sub>2</sub> at such a pH condition (Keenan and Sedlak, 2008). For different secondary metal species, the maximum HCHO levels achieved at different pH and secondary metal contents are shown in Figure 21. As seen, all of the levels were greater than the HCHO achieved by BnZVI. The optimal additive content seemed to depend on the additive species. At pH 6, the optimal additive contents for Pd, Ni, and Ag were 5%, 10%, and 1%, corresponding to 22%, 93% and 87% more HCHO produced than the HCHO level (27 μM) of bare ZVI nanoparticles. It is emphasized that the measurement of HCHO production only provided the information regarding the overall ROS yield. However, the tests could not identify the ROS species. Generally, hydroxyl radicals and ferryl ions, two types of ROS probably produced through Fenton system (Fe<sup>2+</sup> and H<sub>2</sub>O<sub>2</sub>), were able to oxidize methanol to formaldehyde.

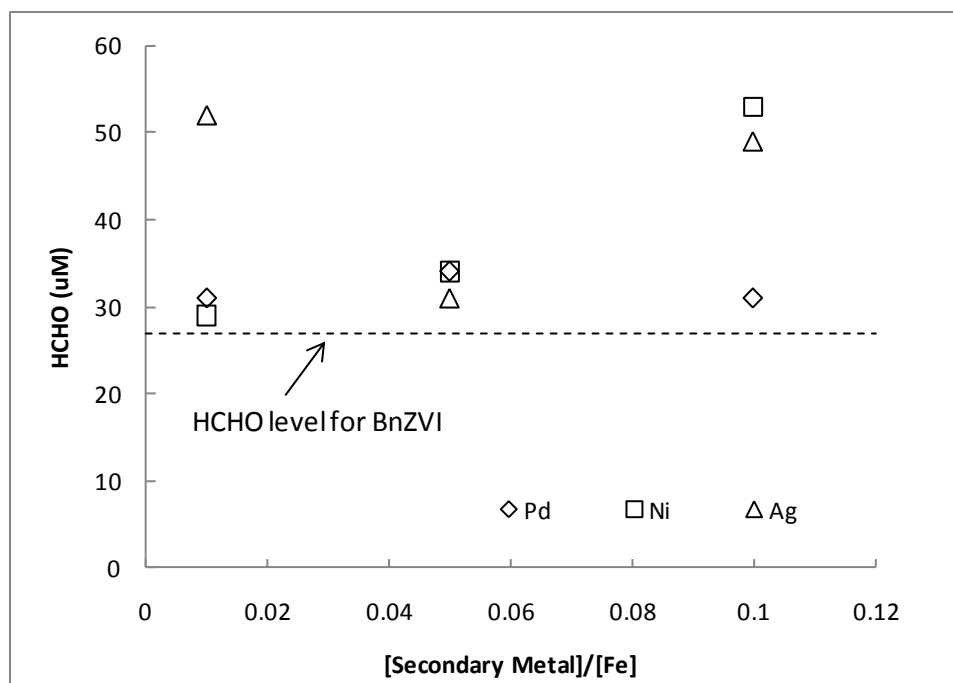


**Figure 21 Comparison of the maximum HCHO production at different pH and secondary metal contents**

#### 4.2.2 Effects of Secondary Metal Content and Solution pH in Hydroxyl Radicals

ROS produced in the nZVI/O<sub>2</sub> system might be hydroxyl radicals or ferryl ions. However, measurement of HCHO, an oxidation product of methanol, could not differentiate the both species. When 2-propanol was used as the probe compound, it was only oxidized by hydroxyl radicals, instead of ferryl ions, to acetone. Therefore, measurement of acetone produced allowed us to quantify the yield of hydroxyl radicals, and to determine the primary oxidant species when the results from 4.2.1 were considered.

The variation of acetone, produced from bare nZVI, over pH 3-9 was shown in Figure 22. The acetone was 23 µM at pH 3, and then peaked (28 µM) at pH 4. With the increasing pH from 4 to 7, acetone was decreased from 28 to 6 µM. At pH 8, the acetone level had a slight increase (11 µM). When pH was increased to 9, acetone dropped to 6 µM. For Pd-Fe nanoparticles, the levels of acetone produced at different pH and Pd contents are shown in Figure 22. Regardless of the Pd content, the Pd-Fe nanoparticles exhibited a similar trend with the bare nZVI over the

studied pH (3-9). The highest levels of acetone occurred at pH 4, except that Pd-Fe nanoparticles with  $[Pd]/[Fe] = 0.10$  had the maximum acetone at pH 3. Furthermore, at any particular pH, the order of acetone produced is roughly as follows:  $[Pd]/[Fe] = 0.01 > 0.10 > 0.05 > \text{bare nZVI}$ .

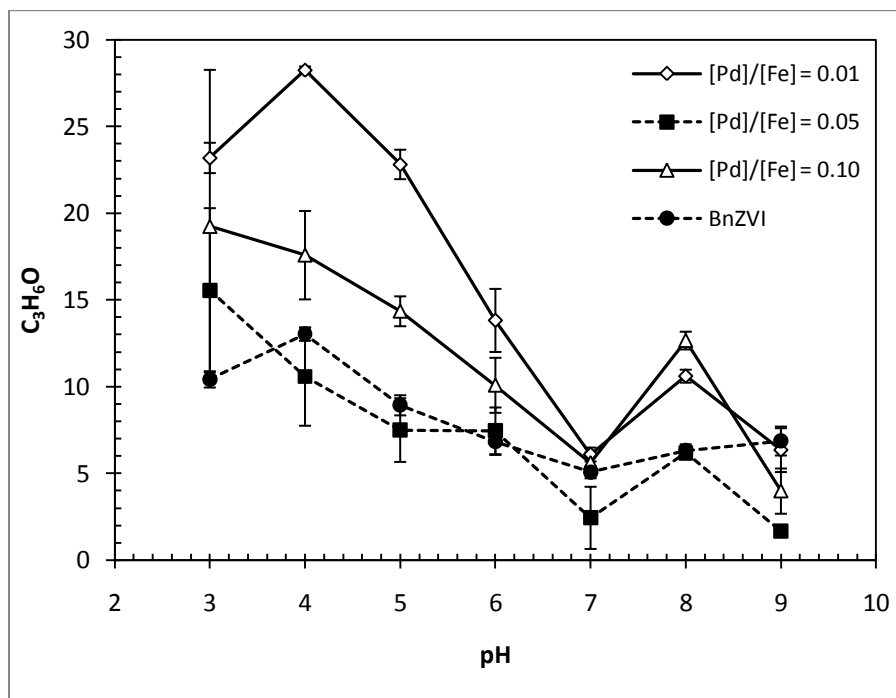


**Figure 22 Production of  $C_3H_6O$  from  $[Pd]/[Fe] = 0.01$ ,  $[Pd]/[Fe] = 0.05$ ,  $[Pd]/[Fe] = 0.10$ . 2-Propanol Initial Concentration =  $250 \mu M$ ;  $[Fe^0] = 400 \mu M$ ; Reaction Time = 180 min**

For Ni-Fe nanoparticles, acetone production at different pH and Ni contents is shown in Figure 23. Interestingly, the acetone curves exhibited different patterns from that produced from Pd-Fe nanoparticles. The acetone levels peaked at pH 7, where the acetone concentrations were 20, 28, and  $25 \mu M$  for  $[Ni]/[Fe] = 0.01$ , 0.05, and 0.10, respectively. No significant difference of acetone production was observed among other pH values. All the acetone levels were greater than those from bare nZVI.

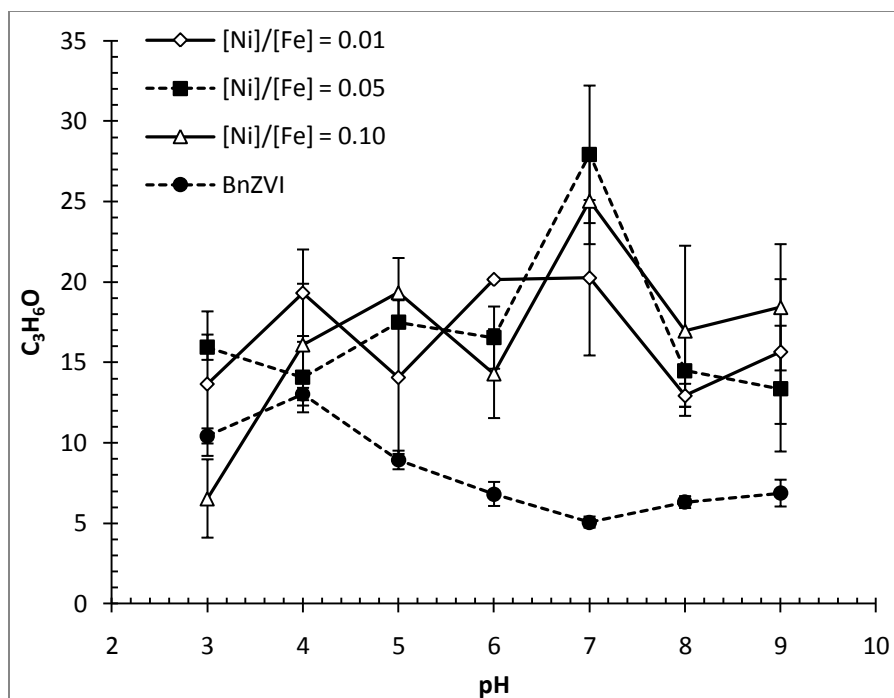


**Figure 23 Production of  $C_3H_6O$  from  $[Ni]/[Fe]= 0.01$ ,  $[Ni]/[Fe] = 0.05$ ,  $[Ni]/[Fe] = 0.10$ . 2-Propanol Initial Concentration =  $250 \mu M$ ;  $[Fe^0] = 400 \mu M$ ; Reaction Time = 180 min**

For Ag-Fe nanoparticles, the levels of acetone produced at different pH and Ag contents are shown in Figure 24. Apparently, Ag-Fe nanoparticles showed similar acetone production behaviors with Pd-Fe nanoparticles. Of note, no significant difference in acetone production was observed for different Ag contents over pH 3-9. At pH4, the maximum acetone levels were  $34 \mu M$ , regardless of the Ag content. All the concentrations of acetone were above that produced from bare nZVI.

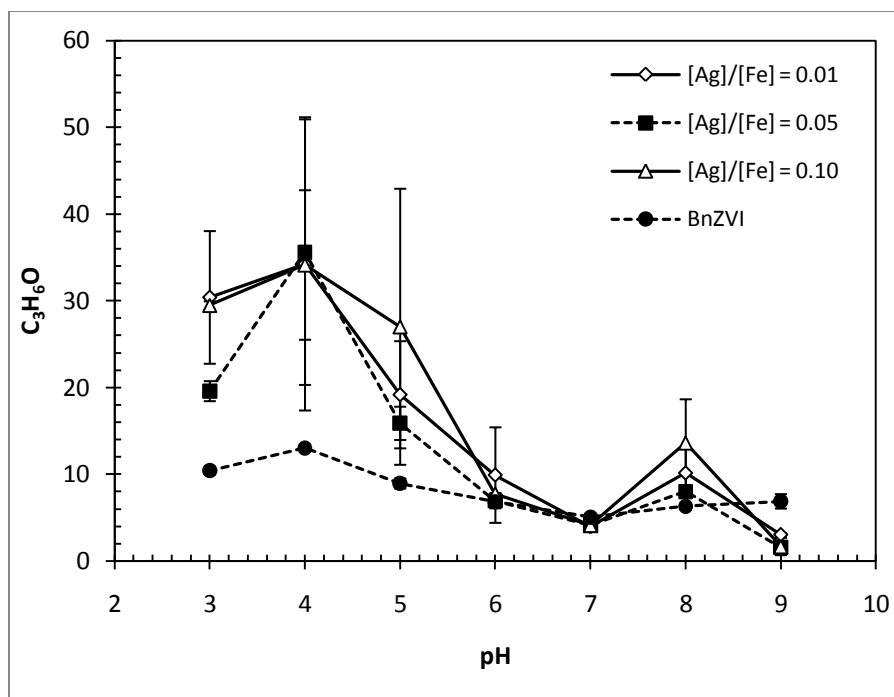


**Figure 24 Production of  $C_3H_6O$  from  $[Ag]/[Fe]= 0.01$ ,  $[Ag]/[Fe] = 0.05$ ,  $[Ag]/[Fe] = 0.10$ . 2-Propanol Initial Concentration =  $250 \mu M$ ;  $[Fe^0] = 400 \mu M$ ; Reaction Time = 180 min**

### 4.3 Track of the Key Intermediates

#### 4.3.1 Production of Ferrous Ion ( $Fe^{2+}$ )

The initial product of nZVI oxidation by  $O_2$  is ferrous iron ( $Fe^{2+}$ ). The variation of  $Fe^{2+}$  over time at pH 4 in bare nZVI/ $O_2$ , Ni-Fe/ $O_2$ , Pd-Fe/ $O_2$ , and Ag-Fe/ $O_2$  systems is shown in Figure 25. At the acidic condition, the  $Fe^{2+}$  level was rapidly produced to  $\sim 150 \mu M$  within 1 min and then slowly increased to  $220 \mu M$  until 60 min in the bare nZVI/ $O_2$  system. Within 180 min,  $Fe^{2+}$  concentration was slightly increased to  $230 \mu M$ , representing  $58\% \pm 0.03$  of the total initial nZVI added.

For the three bimetallic iron nanoparticles, the  $Fe^{2+}$  production showed a similar behavior with bare nZVI. In the Ni-Fe/ $O_2$  system  $167 \mu M Fe^{2+}$  was produced within the first 0.5 min, and then the  $Fe^{2+}$  concentration was increased to  $272 \mu M$  at 180 min. Ni-Fe nanoparticles produced more  $Fe^{2+}$  than bare nZVI, and had the highest ferrous production among the three bimetallic iron/oxygen systems. Pd-Fe/ $O_2$  and Ag-Fe/ $O_2$  systems both showed lower  $Fe^{2+}$  concentration

over the reaction time than nZVI/O<sub>2</sub>. The Pd-Fe/O<sub>2</sub> and Ag-Fe/O<sub>2</sub> produced Fe<sup>2+</sup> concentration ranging from 150.65 to 190 μM and 130.21 to 230.63 μM from 0.5 to 180 min, respectively.

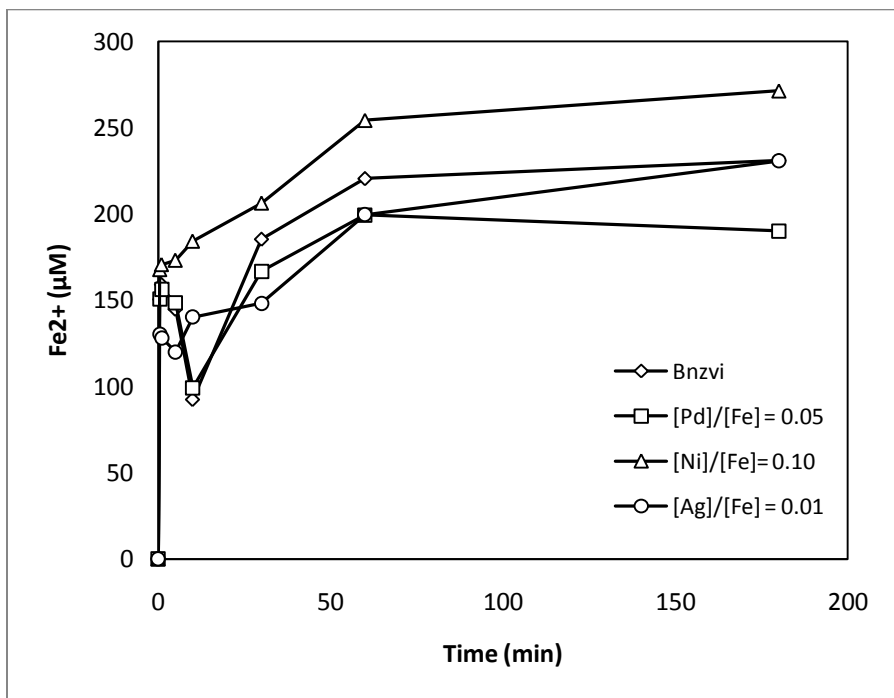


**Figure 25 Production of Ferrous Iron from [Ni]/[Fe]= 0.10, [Pd]/[Fe] = 0.05, [Ag]/[Fe] = 0.01 over time. [Fe<sup>0</sup>] = 400 μM; pH = 4.**

The variation of Fe<sup>2+</sup> over time at pH 6 in bare nZVI/O<sub>2</sub>, Ni-Fe/O<sub>2</sub>, Pd-Fe/O<sub>2</sub>, and Ag-Fe/O<sub>2</sub> systems is shown in Figure 26. Within the first 1 min, the production rates of Fe<sup>2+</sup> were approximately similar to those observed at pH 4 in the bare nZVI/O<sub>2</sub>, Ni-Fe/O<sub>2</sub> and Ag-Fe/O<sub>2</sub>. However, the Pd-Fe/O<sub>2</sub> produced 42 μM at 1 min, much lower than the correspond level of 156 μM at pH 4. After the first min, Fe<sup>2+</sup> in the three bimetallic iron/oxygen systems rapidly decreased, and the remaining Fe<sup>2+</sup> was < 20 μM at 180 min, probably attributable to the oxidation of Fe<sup>2+</sup> by oxygen. In contrast, the Fe<sup>2+</sup> level continuously increased after the 1<sup>st</sup> min, and reached 190 μM at 180 min.

As seen in Figure 26, the lower Fe<sup>2+</sup> level was observed at pH 6 than at pH 4. The reasons may include: (1) Fe<sup>2+</sup> more readily reacts with hydroxide to form solid Fe(OH)<sub>2</sub> at pH 6;

(2)  $\text{Fe}^{2+}$  is more rapidly oxidized by oxygen at pH 6; and (3) more  $\text{Fe}^{2+}$  species was adsorbed to  $\text{Fe}^0$  and  $\text{Fe}^{3+}$  oxyhydroxides formed via  $\text{Fe}^{2+}$  oxidation (Joo et al., 2004).

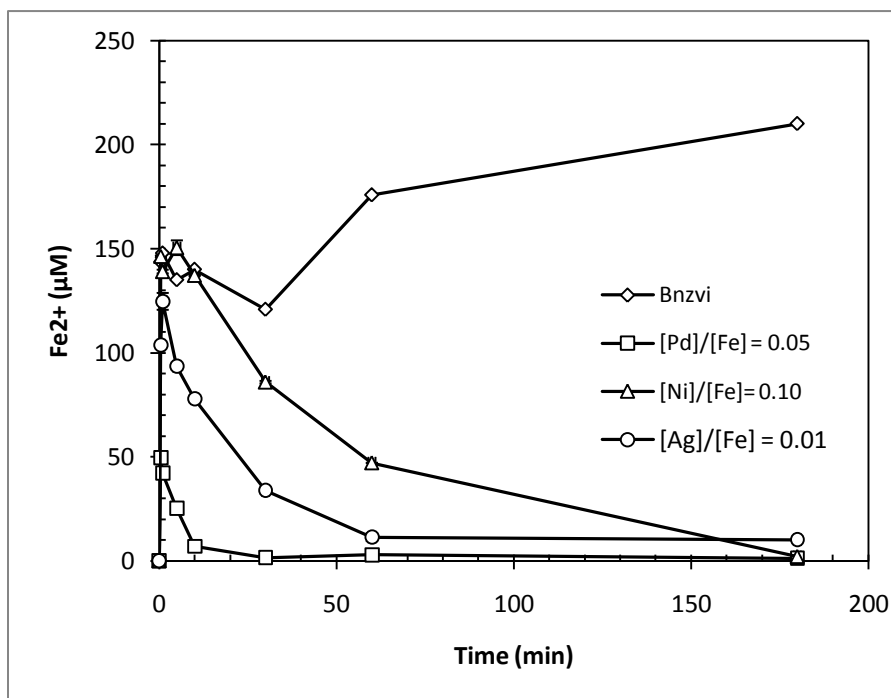


**Figure 26 Production of Ferrous Iron from [Ni]/[Fe]= 0.10, [Pd]/[Fe] = 0.05, [Ag]/[Fe] = 0.01 over time.  $[\text{Fe}^0] = 400 \mu\text{M}$ ; pH = 6**

#### 4.3.2 Production of Hydrogen Peroxide ( $\text{H}_2\text{O}_2$ )

Hydrogen peroxide ( $\text{H}_2\text{O}_2$ ) is the other important intermediate product. The production of  $\text{H}_2\text{O}_2$  at pH 4 under the identical experimental conditions with ferrous measurements is shown in Figure 27. As seen, all the iron nanoparticles in the presence of oxygen rapidly produced  $\text{H}_2\text{O}_2$  within 0.5 min. The  $\text{H}_2\text{O}_2$  concentrations reached 26.05, 49.16, 28.07, and 21.81  $\mu\text{M}$  for bare nZVI, Pd-Fe ( $[\text{Pd}]/[\text{Fe}]=0.05$ ), Ni-Fe ( $[\text{Ni}]/[\text{Fe}]=0.10$ ), and Ag-Fe ( $[\text{Ag}]/[\text{Fe}]=0.01$ ) nanoparticles, respectively. Thereafter,  $\text{H}_2\text{O}_2$  produced from all the nanoparticles slightly increased until 180 min, except Pd-Fe/ $\text{O}_2$  with  $[\text{Pd}]/[\text{Fe}] = 0.05$  whose concentration was reduced to 37.59  $\mu\text{M}$  at 180 min. The highest  $\text{H}_2\text{O}_2$  concentration of 48.55  $\mu\text{M}$  was detected for Ni-Fe/ $\text{O}_2$  at 180 min.

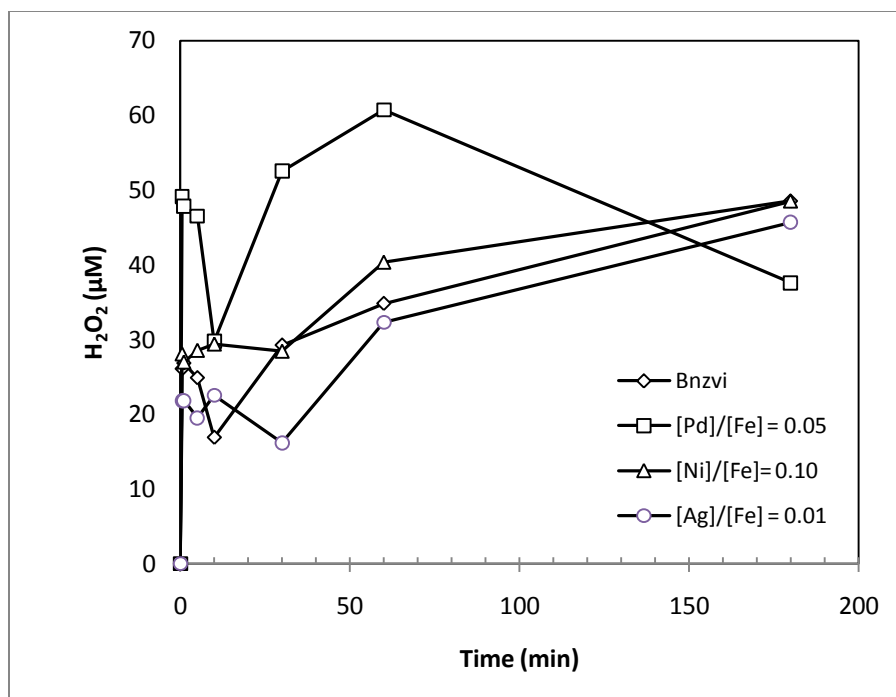


**Figure 27 Production of hydrogen peroxide from [Ni]/[Fe]= 0.10, [Pd]/[Fe] = 0.05, [Ag]/[Fe] = 0.01 over time. [Fe<sup>0</sup>] = 400 μM; pH = 4**

The production of H<sub>2</sub>O<sub>2</sub> at pH 6 under the identical experimental conditions with ferrous measurements is shown in Figure 28. As seen, within 0.5 min, bare nZVI, Pd-Fe ([Pd]/[Fe]=0.05), Ni-Fe ([Ni]/[Fe]=0.10), and Ag-Fe ([Ag]/[Fe]=0.01) nanoparticles rapidly produced 17.62, 9.64, 21.99, and 16.42 μM H<sub>2</sub>O<sub>2</sub>, respectively. The H<sub>2</sub>O<sub>2</sub> levels were lower than their corresponding levels at pH4. Thereafter, the H<sub>2</sub>O<sub>2</sub> concentrations at all the bimetallic iron/oxygen system rapidly decreased. After 180 min, Pd-Fe ([Pd]/[Fe]=0.05), Ni-Fe ([Ni]/[Fe]=0.10), and Ag-Fe ([Ag]/[Fe]=0.01) nanoparticles produced 6.60, 0.75 and 2.71 μM H<sub>2</sub>O<sub>2</sub>, respectively. In contrast, the H<sub>2</sub>O<sub>2</sub> concentration in the bare nZVI/oxygen system decreased to 12.29 μM at 30 min, and then gradually increased with the increasing reaction time. At 180 min, the H<sub>2</sub>O<sub>2</sub> level reached 30.99 μM.

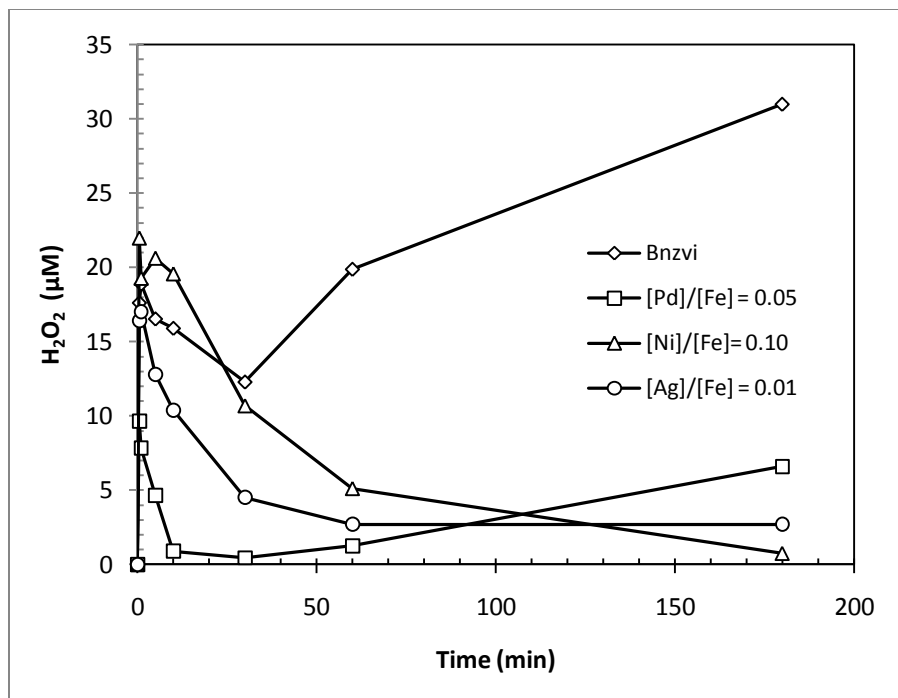


**Figure 28** Production of Hydrogen Peroxide from [Ni]/[Fe]= 0.10, [Pd]/[Fe] = 0.05, [Ag]/[Fe] = 0.01 over time.  $[Fe^0] = 400 \mu M$ ; pH = 6

## 5. DISCUSSION

### 5.1 ROS production at different pH

Under acidic conditions (pH 3-4), the production of oxidant species from Pd-Fe/O<sub>2</sub>, Ni-Fe/O<sub>2</sub> and Ag-Fe/O<sub>2</sub> systems is elucidated in reactions 1, 2, 3 and 7 (pathway 1). Fe<sup>2+</sup> concentrations represent 48%, 68% and 58% for Pd-Fe/O<sub>2</sub>, Ni-Fe/O<sub>2</sub> and Ag-Fe/O<sub>2</sub> systems respectively, of the nZVI initially added. At circumneutral pH (5-7) and higher values, oxidant yields are due to reactions 1, 4, 5 and 7 (pathway 2). The both pathways reflect that Fe<sup>2+</sup> and H<sub>2</sub>O<sub>2</sub> play an important role in the formation of reactive oxidant species.

Apparently, the Fe<sup>2+</sup> oxidation by O<sub>2</sub> is very slow at pH 4 as compared to at pH 6. Under an acidic condition, reactions 1, 2 and 3 are more significant to contribute to H<sub>2</sub>O<sub>2</sub>. Keenan & Sedlak (2008) reported that the ROS yield is consistent with the reduction of oxygen through the two electron transfers on the iron surface studied in reactions 1, 2, 3 and 6. The stoichiometry for these four reactions is 2:1 ([Fe<sup>0</sup>]:[O<sub>2</sub>]), or 0.5 mol O<sub>2</sub> reduced for every mol Fe<sup>0</sup> oxidized. At circumneutral pH, Fe<sup>0</sup> is oxidized to produce Fe<sup>2+</sup> (reaction 1 and 2) followed by Fe<sup>2+</sup> oxidation by oxygen which produces H<sub>2</sub>O<sub>2</sub> to generate oxidants. This is consistent with Fe<sup>2+</sup> concentrations measured in the different systems, where Fe<sup>2+</sup> production increased in the first stage of reaction, then gradually decreased as is oxidized by oxygen.

Fe<sup>2+</sup>, as a key intermediate in the ROS production in nZVI/O<sub>2</sub> and Ni-Fe/O<sub>2</sub> system, was investigated by Lee and Sedlak (2008). Fe<sup>2+</sup> was added to reactors in absence of nZVI or Ni-Fe bimetallic nZVI at the same conditions set in this study. As a result, the yields of HCHO with added Fe<sup>2+</sup> were similar to that with nanoparticles. The yield of HCHO was increased as Fe<sup>2+</sup> was gradually increased. However, at higher Fe<sup>2+</sup> concentrations, the yield of HCHO decreases due to the rapid co-precipitation of Fe<sup>2+</sup> and Fe<sup>3+</sup>. Lee and Sedlak (2008) suggested that slow release of Fe<sup>2+</sup> from Ni-Fe bimetallic nZVI may have limited the co-precipitation of Fe<sup>2+</sup> and Fe<sup>3+</sup> and enhances the yield of ROS. Same characteristics may be occurring in the ROS production in Pd-Fe/O<sub>2</sub> and Ag-Fe/O<sub>2</sub> systems.

Above pH 6, the production of HCHO gradually decreased. This may be attributed in a change in reaction mechanism or ferrous association with a metal or surface. In addition, the low solubility of ferric iron at a basic pH can inhibit the HCHO production (Keenan & Sedlak, 2008).

The addition of Pd, Ni and Ag has an important effect in the enhancement of ROS due to formation of numerous galvanic cells between Fe<sup>0</sup> core and these metal additives on its surface. This contributes to the slow reaction kinetics that occurs in the particle surface (reaction 1 and 2).

As a result of different redox potentials between the metals, electron transfer is enhanced and may produce more Fe<sup>2+</sup> and hydrogen peroxide (H<sub>2</sub>O<sub>2</sub>), two key intermediate products previously described in the reaction mechanism. For example, Lee and Sedlak (2008) studied the Ni-Fe/O<sub>2</sub> system in the ROS enhancement and production. The Ni-Fe bimetallic nanoparticles produced Fe<sup>2+</sup> more slowly over time because of the lower reactivity with O<sub>2</sub> and H<sub>2</sub>O<sub>2</sub> and because of higher redox potential of nickel (E<sup>0</sup> = -0.257 V) than nZVI (E<sup>0</sup> = -0.447 V). Similar effect is probably occurring in Pd-Fe/O<sub>2</sub> and Ag-Fe/O<sub>2</sub> systems, whose redox potential are 0.915 V and 0.799 V, respectively.

In our study, at acidic conditions (~ pH 4), the production of HCHO in Pd-Fe/O<sub>2</sub>, Ni-Fe/O<sub>2</sub> and Ag-Fe/O<sub>2</sub> systems was increased by 11%, 75% and 112%, respectively, than that (14.12 μM) of bare ZVI nanoparticles.. At such pH condition, the production of ROS is controlled by reactions 1-2 and the four electron transfer process. The four electron transfer oxidation occurs through the formation of absorbed H<sub>2</sub>O<sub>2</sub> on the nZVI surface (Jovancicevic & Bockris, 1986, Zecevic & Drazic, 1989; Zecevic et al., 1991). The yield of ROS produced depends on the amount of desorbed H<sub>2</sub>O<sub>2</sub> from the nZVI surface that will react with Fe<sup>2+</sup> already released through the reaction 7. Due to the low reactivity of the bimetallic nanoparticles surface, the generation of absorbed H<sub>2</sub>O<sub>2</sub> is increased, releasing more H<sub>2</sub>O<sub>2</sub> and more oxidants are produced (reaction 7) (Lee and Sedlak, 2008).

The important role of H<sub>2</sub>O<sub>2</sub> in the production of ROS for degradation of herbicide molinate was examined by Joo et al. (2008). Catalase, an enzyme that leads to the decomposition of hydrogen peroxide, was added to air-saturated solutions containing nZVI (10.7 mM and molinate (100 ppb) at pH 6. In the presence of catalase, no molinate degradation was observed

after 3 hrs. The addition of this enzyme scavenged  $\text{H}_2\text{O}_2$  and depleted the ROS production, in the agreement with the proposed reaction pathways

## 5.2 Nature and Identity of ROS

The proposed reaction pathways have considered the Fenton reaction as the primary source for the production of ROS. However, the oxidant species produced from the Fenton reaction ( $\text{Fe}^{2+}$  and  $\text{H}_2\text{O}_2$ ) has been debatable over a few past decades. In a traditional viewpoint, hydroxyl radicals ( $\text{OH}\cdot$ ) have been regarded as the primary oxidizing agent produced from the Fenton system. In contrast, non-radical oxidant such as ferryl ( $\text{Fe}^{4+}$ ) has been proposed (Hug and Leupin, 2003; Englehardt et al., 2007; Keenan and Sedlak, 2008; Lee and Sedlak, 2008). Pignatello et al., (1999) also observed that in photo-Fenton system a mixture of  $\text{OH}\cdot$  and  $\text{Fe}^{4+}$  has been generated at pH 2.8 and only  $\text{OH}\cdot$  at acidic conditions.

In this study, methanol and 2-propanol, two different ROS probe compounds, offered an approach to understand the nature of ROS. HCHO, the oxidation byproduct of methanol with  $\text{OH}\cdot$  or ferryl, indirectly represents the overall ROS level. It was detected over all the pH range and the highest HCHO concentrations were observed at circumneutral pH. On the other side, acetone, the oxidation product of 2-propanol only with  $\text{OH}\cdot$ , reflects the  $\text{OH}\cdot$  level. We found the highest acetone concentration at pH 3 - 4. Based on the observations, we concluded that hydroxyl radicals are the dominant oxidant species for the iron nanoparticle/oxygen system at an acidic condition, and non-radical oxidizing species (most likely ferryl) are the primary oxidant at a circumneutral condition.

## 6. CONCLUSIONS AND RECOMENDATIONS

This study demonstrated that addition of a more stable metal additive to iron nanoparticle surface could increase the ROS yield in the presence of dissolved oxygen. The ROS has a strong oxidative capacity to degrade a variety of aqueous organic pollutants. In addition, with the optimal metal additive content, the nZVI corrosion may be occurring at slower rates. Based on the results obtained in this research, the following are concluded:

- Formaldehyde (HCHO) and acetone, the oxidation products of methanol and 2-propanol, elucidated a clear insight in the production of ROS. The enhancement of ROS is highly dependent of pH solution, secondary metal content and additive. ROS yield was enhanced over the entire pH range with the highest ROS yields approximately at circumneutral pH (5-6). The optimal additive contents for Pd, Ni, and Ag were 5%, 10%, and 1%, corresponding to 22%, 93% and 87% more HCHO produced than the HCHO level (27  $\mu\text{M}$ ) of bare ZVI nanoparticles.
- $\text{Fe}^{2+}$  and hydrogen peroxide ( $\text{H}_2\text{O}_2$ ) play an important role in the production of ROS in the nZVI/ $\text{O}_2$ , Pd-Fe/ $\text{O}_2$ , Ni-Fe/ $\text{O}_2$ , Ag-Fe/ $\text{O}_2$  systems. All the three systems produced  $\text{Fe}^{2+}$  and ( $\text{H}_2\text{O}_2$ ) at acidic and circumneutral conditions. The rate of production of  $\text{Fe}^{2+}$  from  $\text{Fe}^0$  oxidation by oxygen and the rate of absorption and desorption of hydrogen peroxide ( $\text{H}_2\text{O}_2$ ) from nZVI particle surface determine the production of ROS and subsequent enhancement in the different systems.
- Toxicity of the secondary metals in the bimetallic iron nanoparticles should be considered during application. However, the iron hydroxides/oxides produced from the system may greatly immobilize the metals in a subsurface environment
- The addition of secondary metal to the nZVI surface did not change the nature and mechanism pathways for generation of oxidants.

This technology provides a potential pathway to overcome the drawbacks for applications of ZVI/O<sub>2</sub> process in environmental pollution and is expected to become an alternative for traditional remediation methods. However, more study is needed in order to determine the feasibility of ZVI-based oxidation of contaminants. In this manner, the following are recommended:

- The most important step of this technology is the synthesis of nZVI and bimetallic nZVI for generation of ROS. In order to minimize the cost of nZVI, lower concentration of nZVI may be used in future studies.
- More work is needed to examine the treatment efficiency of ZVI/O<sub>2</sub> process in the oxidation different individual pollutants such as PCBs, TCE, dioxins, and arsenic.

## 7. REFERENCES

- Asmus, K. D., Möckel, H., & Henglein, A. (1973). Pulse radiolytic study of the site of OH· radical attack on aliphatic alcohols in aqueous solution. *J. Phys. Chem.* , 77, 1218–1221.
- Bang, S., Korfiatis, G., & Meng, X. (2005). Removal of arsenic from water by zero-valent iron. *Journal of Hazardous Materials* , 121, 61–67.
- Bell, L. S., Devlin, J. F., Gillham, R. W., & Binning, P. J. (2003). A sequential zero valent iron and aerobic biodegradation treatment system for nitrobenzene. *Journal of Contaminant Hydrology* , 66 (3-4), 201-217 .
- Carpenter, E. (2001). Iron nanoparticles as potential magnetic carriers. *J. Magn. Magn. Mater.* , 225, 17.
- Changa, L., Keenan, C., & Sedlak, D. (2008). Polyoxometalate-enhanced oxidation of organic compounds by nanoparticulate zero-valent iron and ferrous ion in the presence of oxygen. 42 (13), 4921–4926.
- Chen, J., Al-Abed, S. R., Ryan, J., & Li, Z. (2001). Effects of pH on dechlorination of trichloroethylene by zero-valent iron. *Journal of Hazardous Materials* , B83, 243–254.
- Choe, S., Chang, Y., Hwang, K., & Khim, J. (2000). Kinetics of reductive denitrification by nanoscale zero-valent iron. *Chemosphere* , 41, 1307.
- Choi, C., Dong, X., & Kim, B. (2001). Characterization of Fe and Co nanoparticles synthesized by chemical vapor condensation. *Scripta Mater* , 44, 2225.
- Cohen, R., & Mercer, J. (1993). *DNAPL Site Evaluation, EPA 600/R-93/022*. U.S. EPA Office of Research and Development.
- Del Bianco, L., Hernando, A., Navarro, E., & Pasquini, L. (1998). Structural configuration and magnetic effects in as-milled and annealed nanocrystalline. *J. Phys.IV Proc.* , 107.
- Doong, R., & Lai, Y. (2005). Dechlorination of tetrachloroethylene by palladized iron in the presence of humic acid. *Water Research* , 39.
- Elliott, D., & Zhang, W. (2001). Field assessment of nanoscale bimetallic particles for groundwater treatment. *Environ. Sci. Technol.* , 35, 4922.
- Englehardt, J., Meeroff, D., Echegoyen, L., Deng, Y., Raymo, F., & Shibata, T. (2007). Oxidation of aqueous EDTA and associated organics and coprecipitation of inorganics by ambient iron-mediated aeration. *Environ. Sci. Technol.* , 41 (1), 270-276.

- EPA. (2001a). A Citizen's Guide to Monitored Natural Attenuation. *EPA 542-F-01-004* . Washington, DC: U.S. EPA Office of Solid Waste and Emergency Response.
- EPA. (2001b). A Citizen's Guide to Permeable Reactive Barriers. *EPA 542-F-01-005* . Office of Solid Waste and Emergency Response.
- EPA. (2001c). A Citizen's Guide to Soil Washing. *EPA 542-F-01-008* . Washington, DC: Office of Solid Waste and Emergency Response.
- EPA. (2001d). A Citizen's Guide to Solvent Extraction. *EPA 542-F-01-009* . Washington, DC: Office of Solid Waste and Emergency Response.
- EPA. (1990). Citizen's Guide To Ground-Water Protection. *EPA 440/6-90-004* . Office of Groundwater Protection. Office Of Water.
- EPA. (2010a). *Compliance and enforcement*. Retrieved Sept 2, 2010, from Cleanup Enforcement, RCRA Cleanup: <http://www.epa.gov/compliance/cleanup/rcra/>
- EPA. (2010b). *Contaminated site clean up information*. Retrieved June 15, 2010, from Remediation Technologies Screening Matrix and Reference Guide, Version 3.0.
- EPA. (2000). Introduction to Phytoremediation. *EPA/600/R-99/107* . Cincinnati, OH: Office of Research and Development.
- EPA. (1996). *Pump-and-Treat Ground-Water Remediation, A Guide for Decision Makers and Practitioners*, *EPA/625/R-95/005*. Cincinnati, OH: U.S. EPA Office of Research and Development.
- EPA. (2010c). *Superfund*. Retrieved Sept 1, 2010, from Basic Information: <http://www.epa.gov/superfund/about.htm>
- EPA. (2010d). *Technology Innovation and Field Services Division, Contaminated Site Cleanup Information*. Retrieved Sept 1, 2010, from Contaminant Focus: <http://www.clu-in.org/contaminantfocus/default.focus/sec/>
- EPA. (2010d). *Technology Innovation and Field Services, Contaminated Site Cleanup Information*. Retrieved Sept 1, 2010, from Contaminant Focus: [http://www.clu-in.org/contaminantfocus/default.focus/sec/chromium\\_VI](http://www.clu-in.org/contaminantfocus/default.focus/sec/chromium_VI)
- Feitz, A., Joo, S., Guan, J., Sun, Q., Sedlak, D., & Waite, T. (2005). Oxidative transformation of contaminants using colloidal zero-valent iron. *Colloids and Surfaces A: Physicochem. Eng. Aspects* , 265, 88–94.

FRTR. (2010, 10 04). *Federal Remediation Technologies Roundtables, Remediation Technologies Screening Matrix and Reference Guide, Version 4.0*. Retrieved 10 04, 2010, from Ground Water Pumping/Pump and Treat: <http://www.frtr.gov/matrix2/section4/4-48.html>

Ghauch, A., C., G., Charef, A., Rima, J., & Martin-Bouyer, M. (2001). Reductive degradation of carbaryl in water by Zero-valent iron. *Chemosphere* , 42, 419-424.

Glavee, G., Klabunde, K., Sorensen, C., & Hadjipanayis, G. (1995). Glavee, G.N., Klabunde, K.J., Sorensen, C., and Hadjipanayis, G.C. *Inorg. Chem.* , 34, 28.

He, F., & Zhao, D. (2008). Hydrodechlorination of trichloroethene using stabilized Fe-Pd nanoparticles: Reaction mechanism and effects of stabilizers, catalysts and reaction conditions. *Applied Catalysis B: Environmental* , 84, 533–540.

He, P., & Zhao, D. (2005). Preparation and characterization of a new class of starch stabilized bimetallic nanoparticles for degradation of chlorinated hydrocarbons in water. *Environ. Sci. Technol.* , 39, 3314.

Hess, W. P., & Tully, F. P. (1989). Hydrogen-atom abstraction from methanol by OH. *methanol by OH.* , 93, 1944–1947.

Huling, S. G., & Pivetz, B. E. (2006). *Engineering Issue: "In-Situ Chemical Oxidation"*. Office of Research and Development, U.S. Environmental protection Agency, EPA/600/R-06/072.

Joo, S., & Zhao, D. (2008). Destruction of lindane and atrazine using stabilized iron nanoparticles under aerobic and anaerobic conditions: Effects of catalyst and stabilizer. *Chemosphere* , 70, 418–425.

Joo, S., Feitz, A., & Waite, T. (2004). Oxidative degradation of the carbothioate herbicide, molinate, using nanoscale zero-valent iron. *Environ. Sci. Technol.* , 38, 2242-2247.

Joo, S., Feitz, A., Sedlak, D. L., & Waite, T. D. (2005). Quantification of the oxidizing capacity of nanoparticulate zero-valent iron. *Environ. Sci. Technol.* , 39, 1263-1268.

Jovancicevic, V., & Bockris, J. O. (1986). The mechanism of oxygen reduction on iron in neutral solutions. *J. Electrochem. Soc.* , 133, 1797–1807.

kanel, S. R., Manning, B., Charlet, L., & Choi, H. (2005). Removal of arsenic(III) from groundwater by nanoscale zero-valent iron. *Environ. Sci. Technol.* , 39, 1291-1298.

Keenan, C., & Sedlak, D. (2008). Factors affecting the yield of oxidants from the reaction of nanoparticulate zero-valent iron and oxygen. *Environ. Sci. Technol.* , 42, 1262–1267.

Keenan, C., & Sedlak, D. (2008). Ligand-enhanced reactive oxidant generation by nanoparticulate zero-valent iron and oxygen. *Environ Sci Technol.* , 42 (18), 6936-6941.

Kenny, J., Barber, N., Hutson, S., Linsey, K., Lovelace, J., & Maupin, M. (2009). Estimated use of water in the United States in 2005 : US Geological Survey. *Circular 1344*, 52 P.

Kim, Y. H., & Carraway, E. R. (2000). Dechlorination of pentachlorophenol by zero valent iron and modified zero valent irons. *Environ. Sci. Technol.* , 34, 2014-2017.

Kim, Y., & Carraway, E. (2000). Dechlorination of pentachlorophenol by zero valent iron and modified zero valent iron. *Environ. Sci. Technol.* , 34 (10), 2014-2017.

Lee, C., & Sedlak, D. (2008). Enhanced formation of oxidants from bimetallic nickel-iron nanoparticles in the presence of oxygen. *Environ. Sci. Technol.* , 42 (22), 8528–8533.

Lee, C., Jee, Y. K., Won, I., K.L., N., Yoon, J., & Sedlak, D. (2008). Bactericidal effect of zero-valent iron nanoparticles on Escherichia coli. *Environmental Science and Technology* , 42 (13), 4927-4933.

Lee, J., Hozalski, R., & Arnold, W. A. (2007). Effects of dissolved oxygen and iron aging on the reduction of trichloronitromethane, trichloroacetonitrile, and trichloropropanone. *Chemosphere* , 66 (11), 2127-2135 .

Li, F., Vipulanandan, C., & Mohanty, K. (2003). Microemulsion and solution approaches to nanoparticle iron production for degradation of trichloroethylene. *Colloid Surf. A: Physicochem. Eng.* , 223, 103.

Li, L., Fan, M., Brown, R., & Van Leeuwen, J. (2006). Synthesis, properties, and environmental applications of nanoscale iron-based materials: a review. *Critical Reviews in Environmental Science and Technology* , 36, 405-431.

Lien, H. L., & Zhang, W. (1999). Transformation of chlorinated methanes by nanoscale iron particles. *Journal of Environmental Engineering* , 125 (11), 1042–1047.

Lien, H., & Zhang, W. (2005). Hydrodechlorination of chlorinated ethanes by nanoscale Pd/Fe bimetallic particles. *Journal of Environmental Engineering, ASCE* , 131 (1), 4-10.

Lien, H., & Zhang, W. (2001). Nanoscale iron particles for complete reduction of chlorinated ethenes. *Colloids and Surfaces A: Physicochemical and Engineering Aspects* , 191, 97–105.

Liu, Y., Majetich, S., Tilton, R., Sholl, D., & Lowry, G. (2005). TCE dechlorination rates, pathways, and efficiency of nanoscale iron particles with different properties. *Environ. Sci. Technol.* , 39, 1338-1345.

Liu, Z., Wang, H., Lu, Q., Du, G., Peng, L., Du, Y., et al. (2004). Synthesis and characterization of ultrafine well-dispersed magnetic nanoparticles. *J. Magn. Magn. Mater.* , 284, 258.

- Lowry, G., & Johnson, K. (2004). Congener-specific dechlorination of dissolved PCBs by microscale and nanoscale zero valent iron in a water/methanol solution. *Environ. Sci. Technol.* , 38, 5208-5216.
- Lu, M., Anotai, J., Liao, C., & Ting, w. (2004). Dechlorination of hexachlorobenzene by zero-valent iron. *Practice Periodical of Hazardous, Toxic, and Radioactive Waste Management ASCE* , 8 (2), 136-140.
- Lu, M., Anotai, J., Liao, C., & Ting, W. (2004). Dechlorination of Hexachlorobenzene by Zero-Valent Iron. *Practice Periodical of Hazardous, Toxic, and Radioactive Waste Management, ASCE* , 136-140.
- Makela, J., Keskinen, H., Forsblom, T., & Keskinen, J. (2004). Generation of metal and metal oxide nanoparticles by liquid flame spray process. *J. Mater. Sci.* , 39, 2783.
- Malow, T., Koch, C., Miraglia, P., & Murty, K. (1998). Compressive mechanical behavior of nanocrystalline Fe investigated with an automated ball indentation technique. *Mater. Sci. Eng.* , A252, 36.
- Matheson, L., & Tratnyek, P. (1994). Reductive dehalogenation of chlorinated methanes by iron metal. *Environmental Technology & Science* , 28 (12), 2045-2053.
- Miller, J., Whitehead, R., & Olcott, P. (1997). *Ground Water Atlas of the United States*.
- Miller, R. (1996). *Air Sparging*. Pittsburg, PA: Ground-Water Remediation Technologies Analysis Center.
- Naja, G., Halasz, A., Thiboutot, S., Ampleman, G., & Hawari, J. (2008). Degradation of hexahydro-1,3,5-trinitro-1,3,5-triazine (RDX) using zero valent iron. *Environ. Sci. Technol.* , 42, 4364–4370.
- Nakayama, T. C. (1998). Nanocrystalline iron oxide manufactured by IGC-PECS process. *Funtai oyobi Funmatsu Yakin* , 45, 1207.
- Natter, H., Schmelzer, M., Loffler, M., Krill, C., Fitch, A., & Hempelmann, R. (2000). Grain-growth kinetics of nanocrystalline iron studied in situ by synchrotron realtime X-ray diffraction. *J. Phys. Chem.* , B104, 2467.
- Noradoun, C. E., & Cheng, F. I. (2005). EDTA degradation induced by oxygen activation in a zerovalent iron/air/water system. *Environmental Science and Technology* , 39 (18), 7158-7163.
- Noradoun, C., Engelmann, M., McLaughlin, M., Hutcheson, R., Breen, K., Paszczynski, A., et al. (2003). Destruction of chlorinated phenols by dioxygen activation under aqueous room temperature and pressure conditions. *Ind. Eng. Chem. Res.* , 42, 5024-5030.

- Nurmi, J., Tratnyek, P., Sarathy, V., Baer, D., & Amonette, J. (2005). Characterization and properties of metallic iron nanoparticles: Spectroscopy, electrochemistry and kinetics. *Environ. Sci. Technol.*, *39*, 1221.
- Nyer, E. K. (1993). *Practical techniques for Groundwater and Soil Remediation*. London: Lewis publishers.
- Pignatello, J. J., Liu, D., & Huston, P. (1999). Evidence for an additional oxidant in the photoassisted Fenton reaction. *Environ. Sci. Technol.*, *33*, 1832–1839.
- Ponder, S., Darab, J. G., & Mallouk, T. (2000). Remediation of Cr(VI) and Pb(II) aqueous solutions using supported, nanoscale zero-valent iron. *Environ. Sci. Technol.*, *34*, 2564-2569.
- Roote, D. (1997). *in Situ flushing*. Pittsburg, PA: groundwater Remediation Technologies Analysis Center.
- Sanchez-Lopez, J., Justo, A., Fernandez, A., Conde, C., & Conde, A. (1997). Preparation and thermal evolution of vapor-condensed nanocrystalline iron. *Philos. Mag. B Phys. Condens. Matter*, *76*, 663.
- Sayles, G. D. (1997). DDT, DDD, and DDE dechlorination by zero-valent iron. *Environ. Sci. Technol.*, *31* (12), 3448–3454.
- Schrick, B., Blough, J., Jones, A., & Mallouk, T. (2002). Hydrodechlorination of trichloroethylene to hydrocarbons using bimetallic nickel-iron nanoparticles. *Chem. Mater.*, *14*, 5140-5147.
- Schrick, B., Hydutsky, B. W., Blough, J. L., & Mallouk, T. E. (2004). Delivery vehicles for zerovalent metal nanoparticles in soil and groundwater. *Chem. Mater.*, *16*, 2187–2193.
- Song, G., Bo, J., & Guo, R. (2004). The characterization and property of polystyrene compounding of  $\alpha$ -Fe<sub>3</sub>O<sub>2</sub> in the nano-scale. *Colloid Polym. Sci.*, *282*, 656.
- Su, C., & Puls, R. W. (2001). Arsenate and arsenite removal by zerovalent iron: kinetics, redox transformation, and implications for in situ groundwater remediation. *Environ. Sci. Technol.*, *35*, 1487-1492.
- Sun, H., Wang, L., Zhang, R., Sui, R., & Xu, G. (2006). Treatment of groundwater polluted by arsenic compounds by zero valent iron. *Journal of Hazardous Materials*, *B129*, 297–303.
- Sus-Ryszkowska, M. W. (Mater. Sci. Eng). Microstructure of ECAP severely deformed iron and its mechanical properties. *A369*, 151.
- Sus-Ryszkowska, M., Wejrzanowski, T., Pakiela, Z., & Kurzydowski, K. (2004). Microstructure of ECAP severely deformed iron and its mechanical properties. *Mater. Sci. Eng.*, *A369*, 151.

- Tao, N., Sui, M., Lu, J., & Lu, K. (1999). Surface nanocrystallization of iron induced by ultrasonic shot peening. *Nano Struc. Mater* , 11, 433.
- Tratnyek, P., & Johnson, R. (2006). Nanotechnologies for environmental cleanup. *Nanotoday* , 1 (2).
- Veve, T., & Taggart, B. (1996). *Atlas of Ground Water Resources in Puerto Rico and the U. S. Virgin Islands*.
- Wang, C., & Zhang, W. (1997). Synthesizing nanoscale iron particles for rapid and complete dechlorination TCE and PEBs. *Environ. Sci. Technol.* , 31, 2154.
- Wiggins, J., Carpenter, E., & O'Connor, C. (2000). Phenomenological magnetic modeling of Au:Fe:Cu nano-onions. *J. Appl. Phys.* , 87, 5651.
- Xu, Y., & Zhang, W. X. (2000). Subcolloidal Fe/Ag particles for reductive dehalogenation of chlorinated benzenes. *Ind. Eng. Chem. Res.* , 39, 2238-2244.
- Yin, Y., & Allen, H. (1999). *In Situ Chemical Treatment*. Pittsburg, PA: Groundwater Remediation Technologies Analysis Center.
- Zecevic, S., & Drazic, D. M. (1989). An analysis of the rotating disk-ring electrode measurements in near neutral solutions. 265, 179–193.
- Zecevic, S., & Drazic, D. M. (1991). Oxygen reduction on iron. Part IV. The reduction of hydrogen peroxide as the intermediate in oxygen reduction reaction in alkaline solutions. *Electrochim. Acta* , 36, 5–14.
- Zhang, W. (2003). Nanoscale iron particles for environmental remediation: An overview. *Journal of Nanoparticle Research* , 5, 323–332.
- Zhang, W. (2003). Nanoscale iron particles for environmental remediation: An overview. *J. Nanoparticle Res.* , 3, 323.